REPORT DOCUMENTATION PAGE

Form Approved
OMB No. 0704-0188

1. AGENCY USE ONLY(Leave blank)	2. REPORT DATE	3. REPORT TYPE AND DATES COVERED
	May, 1996	Technical Report (10/1/94-2/29/96)

4. TITLE AND SUBTITLE
Direct Numerical Simulation for the Receptivity and the Whole Process of Transition Around Joukowsky Airfoils

5. FUNDING NUMBERS
F49620-95-1-0018

6. AUTHOR(S)
Chaoqun Liu
Zhining Liu
Guohua Xiong

7. PERFORMING ORGANIZATION NAME(S) AND ADDRESS(ES)
Department of Mathematics
University of Colorado at Denver
Campus Box 170, P.O. Box 173364
Denver, CO 80217-3364

AFOSR-TR-96
0252

9. SPONSORING/MONITORING AGENCY NAME(S) AND ADDRESS(ES)
AIR FORCE OFFICE OF SCIENTIFIC RESEARCH
DIRECTORATE OF AEROSPACE SCIENCE
BOLLING AFB, DC 20332-6448
N/A

10. SPONSORING/MONITORING AGENCY REPORT NUMBER
95-1-0018

11. SUPPLEMENTARY NOTES

12a. DISTRIBUTION/AVAILABILITY STATEMENT
APPROVED FOR PUBLIC RELEASE
DISTRIBUTION IS UNLIMITED

12b. DISTRIBUTION CODE

19960617 114

13. ABSTRACT *(Maximum 200 words)*

The two- and three- dimensional development of leading-edge receptivity and transition in a 2-D Joukowsky airfoil boundary layer are investigated by direct numerical simulation (DNS) using the incompressible Navier-Stokes equations. The numerical investigation are based on the so-called spatial approach. A contravariant based governing system is derived so that we can simulate the receptivity and transition with complex geometries. The numerical results agreed very well with the experimental results for the flat plate case, and also agreed well with the result obtained by other researchers for the 2-D elliptic leading-edge receptivity case. Some new phenomena for the transition around Joukowsky airfoils were observed which at least qualitatively agree with physics.

14. SUBJECT TERMS	15. NUMBER OF PAGES
direct numerical simulation; multigrid; receptivity; transition; Navier-Stokes equation; implicit	44
	16. PRICE CODE

17. SECURITY CLASSIFICATION OF REPORT	18. SECURITY CLASSIFICATION OF THIS PAGE	19. SECURITY CLASSIFICATION OF ABSTRACT	20. LIMITATION OF ABSTRACT
Unclassified	Unclassified	Unclassified	UL

NSN 7540-01-280-5500

Standard Form 298(Rev. 2-89)
Prescribed by ANSI Std. Z39-18
298-102

☆U.S. GOVERNMENT PRINTING OFFICE: 1994 - 528-064/23021

Direct Numerical Simulation for the Receptivity and the Whole Process of Transition Around Joukowsky Airfoils

Chaoqun Liu, Zhining Liu, and Guohua Xiong
Numerical Simulation Group
University of Colorado at Denver
Campus Box 170, P.O. Box 173364
Denver, CO 80217-3364

Abstract

The two- and three- dimensional development of leading-edge receptivity and transition in a 2-D Joukowsky airfoil boundary layer are investigated by direct numerical simulation (DNS) using the incompressible Navier-Stokes equations. The numerical investigation are based on the so-called spatial approach. A contravariant based governing system is derived so that we can simulate the receptivity and transition with complex geometries. The numerical results agreed very well with the experimental results for the flat plate case, and also agreed well with the result obtained by other researchers for the 2-D elliptic leading-edge receptivity case. Some new phenomena for the transition around Joukowsky airfoils were observed which at least qualitatively agree with physics.

Contents

1 Introduction 1

2 Governing System 2

2.1 Basic state 4

2.2 Perturbation form 8

3 Conformal Mapping 13

3.1 Conformal mapping for a quarter of cylinder 14

3.2 Conformal mapping for the leading-edge flat-plate juncture 16

3.3 Conformal mapping for Joukowsky airfoil 17

4 Numerical Process 20

5 Computational Results 21

5.1 Code validation 21

5.1.1 Linear stage 21

5.1.2 Whole process of transition over a smooth flat plate 22

5.2 Receptivity of flat-plate with an elliptic leading-edge 23

5.3 Receptivity of 2D and 3D Joukowsky airfoils 24

5.4 The whole process of transition around 3D Joukowsky airfoils 26

5.4.1 Enforced transition 26

5.4.2 Natural transition 27

6 Concluding Remarks 42

7 Acknowledgment 42

References 42

Direct Numerical Simulation for the Receptivity and the Whole Process of Transition Around Joukowsky Airfoils

Chaoqun Liu, Zhining Liu, and Guohua Xiong
Numerical Simulation Group
University of Colorado at Denver
Campus Box 170, P.O. Box 173364
Denver, CO 80217-3364

1 Introduction

To understand the origins of transition and turbulence remains a critical problem of fluid mechanics. Important sources of information regarding applications of transition, for example, the design of laminar flow control systems to delay or even eliminate boundary layer transition and to increase the aerodynamic performance of the systems, can be found in a variety of recent literatures (e.g., AGARD Report No.786, 1992; No.793, 1993). Receptivity, the process through which external disturbances generate instability waves in boundary layer (Morkovin, 1969), provides the vital initial conditions of amplitude, phase, frequency, and wavelength for the breakdown of laminar flow. Clearly, the study of receptivity promises significant advances in practical transition prediction methods. This has been the subject at the first stage of our project.

The process of boundary layer transition can be qualitatively described as the following scenario: receptivity to freestream disturbances, initial growth of instability waves, three-dimensional and nonlinear effects coming into play and thus leading to breakdown to turbulence (Saric & Reed, 1994). As briefly reviewed by Liu, Liu & McCormick (1993), considerable progress has been achieved with theoretical, computational, and experimental tools on broadening our knowledge of the latter two stages of transition for boundary layer in the last two decades. However, efforts on understanding the mechanism of receptivity are still quite limited. Mathematically speaking, receptivity problem differs from the stability analysis, which describes the normal modes (eigenvalues) of disturbances determined from the linearized N-S equations, due to the fact that its governing system being typically the full N-S system with appropriate boundary and initial conditions. Because of the system's inherent susceptivity to many subtle environment influences, receptivity theory remains rather incomplete with regarding to quantitative predications of the strength of the disturbances introduced into the boundary. Well-documented experiment data in this area are also limited. DNSs, on the other hand, are playing increasingly important role

in the investigation of transition with the recent progress made in the development of extremely powerful computers and numerical algorithms (Reed, 1993, and Kleiser & Zang, 1991). It is mentionable that significant achievements in spatial DNS have been made by Liu, Liu & McCormick (1991,1992,1993), and Liu & Liu (1993,1994,1995) with the support of NASA Langley Research Center for 1990–1994 and US AFOSR for 1994–present. Our former and present DNS researches have established a viable framework for the study of boundary layer receptivity.

Among various paths through which external energy is internalized in form of instability waves in the boundary layers, such as curvature, sweep, roughness, freestream disturbance, and surface pressure gradient, we choose to consider the receptivity to freestream vortical disturbances of boundary layer flows which include the boundary layer flow over a semi-infinite flat plate with an elliptic leading-edge, and that over a Joukowsky airfoil. This is referred to as leading-edge receptivity. Related works have been performed by Lin, Reed & Saric (1992), and Buter & Reed (1994) which showed the clear appearance of the T-S modes in the boundary layer over a two-dimensional semi-infinite flat plate with elliptic leading-edge of different aspect ratio and some other modified geometries. Receptivity to freestream spanwise vorticity is found to be different for two cases considered: symmetric and asymmetric forcing of the same strength of input disturbances. For the present work, the main purpose is to validate the capability of our new spatial DNS code which is motivated for further studies of real time-dependent three-dimensional compressible turbulent flows around Air Force flight vehicles (the preliminary study is limited to incompressible transitional flow). We first study the receptivity of Joukowsky airfoil to freestream vortical disturbances. So far, all numerical studies on receptivity are limited to 2-D simple geometry, and serve for the purpose of the receptivity study. This work is a first try to study receptivity for 3-D and more general configurations. Finally, we investigated the whole process of flow transition around Joukowsky airfoils.

2 Governing System

The 3-D incompressible time-dependent Navier-Stokes equations are considered as the governing system in this work. On the general curvilinear coordinate system (ξ, η, ζ), these equations can be expressed as follows:

$$\frac{1}{J}\frac{\partial u}{\partial t} + \frac{\partial Uu}{\partial \xi} + \frac{\partial Vu}{\partial \eta} + \frac{\partial Wu}{\partial \zeta} + \frac{1}{J}(\xi_x \frac{\partial}{\partial \xi} + \eta_x \frac{\partial}{\partial \eta} + \zeta_x \frac{\partial}{\partial \zeta})P - \frac{1}{JRe}\Delta_1 u = 0, \quad (1)$$

$$\frac{1}{J}\frac{\partial v}{\partial t} + \frac{\partial Uv}{\partial \xi} + \frac{\partial Vv}{\partial \eta} + \frac{\partial Wv}{\partial \zeta} + \frac{1}{J}(\xi_y \frac{\partial}{\partial \xi} + \eta_y \frac{\partial}{\partial \eta} + \zeta_y \frac{\partial}{\partial \zeta})P - \frac{1}{JRe}\Delta_1 v = 0, \quad (2)$$

$$\frac{1}{J}\frac{\partial w}{\partial t}+\frac{\partial Uw}{\partial \xi}+\frac{\partial Vw}{\partial \eta}+\frac{\partial Ww}{\partial \zeta}+\frac{1}{J}(\xi_z\frac{\partial}{\partial \xi}+\eta_z\frac{\partial}{\partial \eta}+\zeta_z\frac{\partial}{\partial \zeta})P-\frac{1}{JRe}\Delta_1 w = 0, \quad (3)$$

$$\frac{\partial U}{\partial \xi}+\frac{\partial V}{\partial \eta}+\frac{\partial W}{\partial \zeta} = 0, \quad (4)$$

where

$$U=\frac{1}{J}(u\xi_x+v\xi_y+w\xi_z), \quad (5)$$

$$V=\frac{1}{J}(u\eta_x+v\eta_y+w\eta_z), \quad (6)$$

$$W=\frac{1}{J}(u\zeta_x+v\zeta_y+w\zeta_z), \quad (7)$$

and

$$\begin{aligned}
J &= \frac{\partial(\xi,\eta,\zeta)}{\partial(x,y,z)},\\
\frac{1}{J}\Delta_1 &= \alpha\frac{\partial^2}{\partial\xi^2}+\beta\frac{\partial^2}{\partial\eta^2}+\gamma\frac{\partial^2}{\partial\zeta^2}+\\
&\quad 2\lambda_1\frac{\partial^2}{\partial\xi\partial\eta}+2\lambda_3\frac{\partial^2}{\partial\xi\partial\zeta}+2\lambda_2\frac{\partial^2}{\partial\eta\partial\zeta}+\sigma_1\frac{\partial}{\partial\xi}+\sigma_2\frac{\partial}{\partial\eta}+\sigma_3\frac{\partial}{\partial\zeta},\\
\alpha &= \frac{1}{J}(\xi_x^2+\xi_y^2+\xi_z^2),\\
\beta &= \frac{1}{J}(\eta_x^2+\eta_y^2+\eta_z^2),\\
\gamma &= \frac{1}{J}(\zeta_x^2+\zeta_y^2+\zeta_z^2),\\
\lambda_1 &= \frac{1}{J}(\xi_x\eta_x+\xi_y\eta_y+\xi_z\eta_z),\\
\lambda_2 &= \frac{1}{J}(\eta_x\zeta_x+\eta_y\zeta_y+\eta_z\zeta_z),\\
\lambda_3 &= \frac{1}{J}(\xi_x\zeta_x+\xi_y\zeta_y+\xi_z\zeta_z),\\
\sigma_1 &= \frac{1}{J}(\xi_{xx}+\xi_{yy}+\xi_{zz}),\\
\sigma_2 &= \frac{1}{J}(\eta_{xx}+\eta_{yy}+\eta_{zz}),\\
\sigma_3 &= \frac{1}{J}(\zeta_{xx}+\zeta_{yy}+\zeta_{zz}).
\end{aligned} \quad (8)$$

Unfortunately, equations (1)–(3) can cause some trouble for the numerical simulation when the perpendicularity of $U-$, $V-$ and $W-$ are fairly poor. In order to give a system with better behavior, we reorganize them to get equations along $U-$, $V-$, and $W-$ directions, and named them as $U-$momentum, $V-$momentum, and $W-$momentum equations. There are two ways to obtain the discretized system:

1. Obtain the $U-$, $V-$, and $W-$ equations analytically, then discretize them, or

2. Discretize equations (1)-(3) first, and then combine them to obtain the discretized $U-$, $V-$, and $W-$ equations.

In the first way, a non-derivative term will be generated in each momentum equation which makes the conservation of system very poor, and sometimes it is difficult to maintain the zero residual requirement of the momentum equations for the uniform flow field. Therefore, we choose the second way.

To minimize the effects of machine's round-off error, we decompose the total flow into two parts: base flow and perturbation.

2.1 Basic state

Using the second-order central difference as an example, we show how to derive the discretized governing system. First, we discretize (1)–(3) as follows (see Figure 1)

$$\begin{aligned}
&(\frac{1}{J}\frac{\partial u}{\partial t})_{ijk} + \frac{U_e u_e - U_w u_w}{\Delta\xi} + \frac{V_n u_n - V_s u_s}{\Delta\eta} + \frac{W_f u_f - W_b u_b}{\Delta\zeta} \\
&\quad +[\frac{1}{J}(\xi_x\frac{\partial}{\partial\xi} + \eta_x\frac{\partial}{\partial\eta} + \zeta_x\frac{\partial}{\partial\zeta})P]_{ijk} - (\frac{1}{J}\frac{1}{Re}\Delta_1 u)_{ijk} = 0, \qquad (9)\\
&(\frac{1}{J}\frac{\partial v}{\partial t})_{ijk} + \frac{U_e v_e - U_w v_w}{\Delta\xi} + \frac{V_n v_n - V_s v_s}{\Delta\eta} + \frac{W_f v_f - W_b v_b}{\Delta\zeta} \\
&\quad +[\frac{1}{J}(\xi_y\frac{\partial}{\partial\xi} + \eta_y\frac{\partial}{\partial\eta} + \zeta_y\frac{\partial}{\partial\zeta})P]_{ijk} - (\frac{1}{J}\frac{1}{Re}\Delta_1 v)_{ijk} = 0, \qquad (10)\\
&(\frac{1}{J}\frac{\partial w}{\partial t})_{ijk} + \frac{U_e w_e - U_w w_e}{\Delta\xi} + \frac{V_n w_n - V_s w_s}{\Delta\eta} + \frac{W_f w_f - W_b w_b}{\Delta\zeta} \\
&\quad +[\frac{1}{J}(\xi_z\frac{\partial}{\partial\xi} + \eta_z\frac{\partial}{\partial\eta} + \zeta_z\frac{\partial}{\partial\zeta})P]_{ijk} - (\frac{1}{J}\frac{1}{Re}\Delta_1 w)_{ijk} = 0. \qquad (11)
\end{aligned}$$

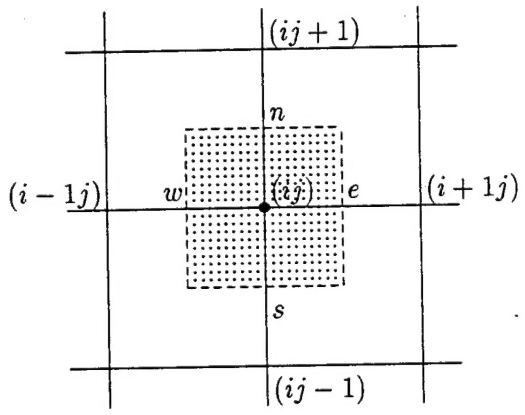

Figure 1. Stencil in the (ξ, η) plane.

To derive the U-equation, using $\xi_{x_{ijk}} \times (9) + \xi_{y_{ijk}} \times (10) + \xi_{z_{ijk}} \times (11)$, and assuming u, v, w are defined everywhere, we obtain:

time term:

$$(\frac{\partial U}{\partial t})_{ijk},$$

$\xi-$direction convection:

$$\frac{J_e U_e U_e - J_w U_w U_w}{\Delta\xi} + \frac{1}{\Delta\xi}\{U_e[u_e(\xi_{x_{ijk}} - \xi_{x_e}) + v_e(\xi_{y_{ijk}} - \xi_{y_e}) + w_e(\xi_{z_{ijk}} - \xi_{z_e})] - U_w[u_w(\xi_{x_{ijk}} - \xi_{x_w}) + v_w(\xi_{y_{ijk}} - \xi_{y_w}) + w_w(\xi_{z_{ijk}} - \xi_{z_w})]\},$$

$\eta-$direction convection:

$$\frac{J_n U_n V_n - J_s U_s V_s}{\Delta\eta} + \frac{1}{\Delta\eta}\{V_n[u_n(\xi_{x_{ijk}} - \xi_{x_n}) + v_n(\xi_{y_{ijk}} - \xi_{y_n}) + w_n(\xi_{z_{ijk}} - \xi_{z_n})] - V_s[u_s(\xi_{x_{ijk}} - \xi_{x_s}) + v_s(\xi_{y_{ijk}} - \xi_{y_s}) + w_s(\xi_{z_{ijk}} - \xi_{z_s})]\},$$

$\zeta-$direction convection:

$$\frac{J_f U_f W_f - J_b U_b W_b}{\Delta\zeta} + \frac{1}{\Delta\zeta}\{W_f[u_f(\xi_{x_{ijk}} - \xi_{x_f}) + v_f(\xi_{y_{ijk}} - \xi_{y_f}) + w_f(\xi_{z_{ijk}} - \xi_{z_f})] - W_b[u_b(\xi_{x_{ijk}} - \xi_{x_b}) + v_b(\xi_{y_{ijk}} - \xi_{y_b}) + w_b(\xi_{z_{ijk}} - \xi_{z_b})]\},$$

Pressure term:

$$\{\alpha\frac{\partial P}{\partial\xi} + \lambda_1\frac{\partial P}{\partial\eta} + \lambda_3\frac{\partial P}{\partial\zeta}\}_{ijk},$$

Viscous term:

$$\begin{aligned}
& (\xi_x\frac{1}{J}\Delta_1 u + \xi_y\frac{1}{J}\Delta_1 v + \xi_z\frac{1}{J}\Delta_1 w)_{ijk} \\
= \; & \{\xi_{x_{ijk}}\frac{u_{i+1jk} - 2u_{ijk} + u_{i-1jk}}{\Delta\xi^2} + \xi_{y_{ijk}}\frac{v_{i+1jk} - 2v_{ijk} + v_{i-1jk}}{\Delta\xi^2} + \\
& \xi_{z_{ijk}}\frac{w_{i+1jk} - 2w_{ijk} + w_{i-1jk}}{\Delta\xi^2}\}\alpha_{ijk} + \\
& \{\xi_{x_{ijk}}\frac{u_{ij+1k} - 2u_{ijk} + u_{ij-1k}}{\Delta\eta^2} + \xi_{y_{ijk}}\frac{v_{ij+1k} - 2v_{ijk} + v_{ij-1k}}{\Delta\eta^2} + \\
& \xi_{z_{ijk}}\frac{w_{ij+1k} - 2w_{ijk} + w_{ij-1k}}{\Delta\eta^2}\}\beta_{ijk} + \\
& \{\xi_{x_{ijk}}\frac{u_{ijk+1} - 2u_{ijk} + u_{ijk-1}}{\Delta\zeta^2} + \xi_{y_{ijk}}\frac{v_{ijk+1} - 2v_{ijk} + v_{ijk-1}}{\Delta\zeta^2} + \\
& \xi_{z_{ijk}}\frac{w_{ijk+1} - 2w_{ijk} + w_{ijk-1}}{\Delta\zeta^2}\}\gamma_{ijk} +
\end{aligned}$$

$$
\begin{aligned}
& \xi_{x_{ijk}} S_{1_{ijk}} + \xi_{y_{ijk}} S_{2_{ijk}} + \xi_{z_{ijk}} S_{3_{ijk}} \\
= \; & \alpha_{ijk} \frac{J_{i+1jk} U_{i+1jk} - 2 J_{ijk} U_{ijk} + J_{i-1jk} U_{i-1jk}}{\Delta \xi^2} + \\
& \frac{\alpha_{ijk}}{\Delta \xi^2} \{ u_{i+1jk} (\xi_{x_{ijk}} - \xi_{x_{i+1jk}}) + u_{i-1jk} (\xi_{x_{ijk}} - \xi_{x_{i-1jk}}) + \\
& v_{i+1jk} (\xi_{y_{ijk}} - \xi_{y_{i+1jk}}) + v_{i-1jk} (\xi_{y_{ijk}} - \xi_{y_{i-1jk}}) + \\
& w_{i+1jk} (\xi_{z_{ijk}} - \xi_{z_{i+1jk}}) + w_{i-1jk} (\xi_{z_{ijk}} - \xi_{z_{i-1jk}}) \} + \\
& \beta_{ijk} \frac{J_{ij+1k} U_{ij+1k} - 2 J_{ijk} U_{ijk} + J_{ij-1k} U_{ij-1k}}{\Delta \eta^2} + \\
& \frac{\beta_{ijk}}{\Delta \eta^2} \{ u_{ij+1k} (\xi_{x_{ijk}} - \xi_{x_{ij+1k}}) + u_{ij-1k} (\xi_{x_{ijk}} - \xi_{x_{ij-1k}}) + \\
& v_{ij+1k} (\xi_{y_{ijk}} - \xi_{y_{ij+1k}}) + v_{ij-1k} (\xi_{y_{ijk}} - \xi_{y_{ij-1k}}) + \\
& w_{ij+1k} (\xi_{z_{ijk}} - \xi_{z_{ij+1k}}) + w_{ij-1k} (\xi_{z_{ijk}} - \xi_{z_{ij-1k}}) \} + \\
& \gamma_{ijk} \frac{J_{ijk+1} U_{ijk+1} - 2 J_{ijk} U_{ijk} + J_{ijk-1} U_{ijk-1}}{\Delta \zeta^2} + \\
& \frac{\gamma_{ijk}}{\Delta \zeta^2} \{ u_{ijk+1} (\xi_{x_{ijk}} - \xi_{x_{ijk+1}}) + u_{ijk-1} (\xi_{x_{ijk}} - \xi_{x_{ijk-1}}) + \\
& v_{ijk+1} (\xi_{y_{ijk}} - \xi_{y_{ijk+1}}) + v_{ijk-1} (\xi_{y_{ijk}} - \xi_{y_{ijk-1}}) + \\
& w_{ijk+1} (\xi_{z_{ijk}} - \xi_{z_{ijk+1}}) + w_{ijk-1} (\xi_{z_{ijk}} - \xi_{z_{ijk-1}}) \} + \\
& \xi_{x_{ijk}} S_{1_{ijk}} + \xi_{y_{ijk}} S_{2_{ijk}} + \xi_{z_{ijk}} S_{3_{ijk}},
\end{aligned}
$$

where

$$
\begin{aligned}
S_1 &= 2\lambda_1 \frac{\partial^2 u}{\partial \xi \partial \eta} + 2\lambda_3 \frac{\partial^2 u}{\partial \xi \partial \zeta} + 2\lambda_2 \frac{\partial^2 u}{\partial \eta \partial \zeta} + \sigma_1 \frac{\partial u}{\partial \xi} + \sigma_2 \frac{\partial u}{\partial \eta} + \sigma_3 \frac{\partial u}{\partial \zeta}, \\
S_2 &= 2\lambda_1 \frac{\partial^2 v}{\partial \xi \partial \eta} + 2\lambda_3 \frac{\partial^2 v}{\partial \xi \partial \zeta} + 2\lambda_2 \frac{\partial^2 v}{\partial \eta \partial \zeta} + \sigma_1 \frac{\partial v}{\partial \xi} + \sigma_2 \frac{\partial v}{\partial \eta} + \sigma_3 \frac{\partial v}{\partial \zeta}, \\
S_3 &= 2\lambda_1 \frac{\partial^2 w}{\partial \xi \partial \eta} + 2\lambda_3 \frac{\partial^2 w}{\partial \xi \partial \zeta} + 2\lambda_2 \frac{\partial^2 w}{\partial \eta \partial \zeta} + \sigma_1 \frac{\partial w}{\partial \xi} + \sigma_2 \frac{\partial w}{\partial \eta} + \sigma_3 \frac{\partial w}{\partial \zeta}.
\end{aligned}
$$

Similarly, we can use $\eta_{x_{ijk}} \times (9) + \eta_{y_{ijk}} \times (10) + \eta_{z_{ijk}} \times (11)$ to obtain V-equation, and $\zeta_{x_{ijk}} \times (9) + \zeta_{y_{ijk}} \times (10) + \zeta_{z_{ijk}} \times (11)$ to obtain W-equation. The resulting discretized system can now be written as follows:

$$
\begin{aligned}
\frac{U_{ijk} - U^n_{ijk}}{\Delta t} + & \frac{J_e U_e (U_{ijk} + U_{i+1jk}) - J_w U_w (U_{ijk} + U_{i-1jk})}{2\Delta \xi} + \\
& \frac{J_n V_n (U_{ijk} + U_{ij+1k}) - J_s V_s (U_{ijk} + U_{ij-1k})}{2\Delta \eta} + \\
& \frac{J_f W_f (U_{ijk} + U_{ijk+1}) - J_b W_b (U_{ijk} + U_{ijk-1})}{2\Delta \zeta} +
\end{aligned}
$$

$$\alpha_{ijk}\frac{P_e - P_w}{\Delta\xi} - \frac{1}{Re}\{\alpha_{ijk}\frac{J_{i+1jk}U_{i+1jk} - 2J_{ijk}U_{ijk} + J_{i-1jk}U_{i-1jk}}{\Delta\xi^2} +$$
$$\beta_{ijk}\frac{J_{ij+1k}U_{ij+1k} - 2J_{ijk}U_{ijk} + J_{ij-1k}U_{ij-1k}}{\Delta\eta^2} +$$
$$\gamma_{ijk}\frac{J_{ijk+1}U_{ijk+1} - 2J_{ijk}U_{ijk} + J_{ijk-1}U_{ijk-1}}{\Delta\zeta^2}\}$$
$$+S_{CONV_{ijk}}(\xi) + S_{VIS_{ijk}}(\xi) + \lambda_{1_{ijk}}\frac{P_n - P_s}{\Delta\eta} + \lambda_{3_{ijk}}\frac{P_f - P_b}{\Delta\zeta}$$
$$-\frac{1}{Re}\{\xi_{x_{ijk}}S_{1_{ijk}} + \xi_{y_{ijk}}S_{2_{ijk}} + \xi_{z_{ijk}}S_{3_{ijk}}\} = 0, \qquad (12)$$
$$\frac{V_{ijk} - V^n_{ijk}}{\Delta t} + \frac{J_eU_e(V_{i+1jk} + V_{ijk}) - J_wU_w(V_{i-1jk} + V_{ijk})}{2\Delta\xi} +$$
$$\frac{J_nV_n(V_{ijk} + V_{ij+1k}) - J_sV_s(V_{ijk} + V_{ij-1k})}{2\Delta\eta} +$$
$$\frac{J_fW_f(V_{ijk} + V_{ijk+1}) - J_bW_b(V_{ijk} + V_{ijk-1})}{2\Delta\zeta} +$$
$$\beta_{ijk}\frac{P_n - P_s}{\Delta\eta} - \frac{1}{Re}\{\alpha_{ijk}\frac{J_{i+1jk}V_{i+1jk} - 2J_{ijk}V_{ijk} + J_{i-1jk}V_{i-1jk}}{\Delta\xi^2} +$$
$$\beta_{ijk}\frac{J_{ij+1k}V_{ij+1k} - 2J_{ijk}V_{ijk} + J_{ij-1k}V_{ij-1k}}{\Delta\eta^2} +$$
$$\gamma_{ijk}\frac{J_{ijk+1}V_{ijk+1} - 2J_{ijk}V_{ijk} + J_{ijk-1}V_{ijk-1}}{\Delta\zeta^2}\}$$
$$+\lambda_{1_{ijk}}\frac{P_e - P_w}{\Delta\xi} + \lambda_{2_{ijk}}\frac{P_f - P_b}{\Delta\zeta} + S_{CONV_{ijk}}(\eta) + S_{VIS_{ijk}}(\eta)$$
$$-\frac{1}{Re}\{\eta_{x_{ijk}}S_{1_{ijk}} + \eta_{y_{ijk}}S_{2_{ijk}} + \eta_{z_{ijk}}S_{3_{ijk}}\} = 0, \qquad (13)$$
$$\frac{W_{ijk} - W^n_{ijk}}{\Delta t} + \frac{J_eU_e(W_{i+1jk} + W_{ijk}) - J_wU_w(W_{i-1jk} + W_{ijk})}{2\Delta\xi} +$$
$$\frac{J_nV_n(W_{ij+1k} + W_{ijk}) - J_sV_s(W_{ij-1k} + W_{ijk})}{2\Delta\eta} +$$
$$\frac{J_fW_f(W_{ijk+1} + W_{ijk}) - J_bW_b(W_{ijk-1} + W_{ijk})}{2\Delta\eta} +$$
$$\gamma_{ijk}\frac{P_f - P_b}{\Delta\zeta} - \frac{1}{Re}\{\alpha_{ijk}\frac{J_{i+1jk}W_{i+1jk} - 2J_{ijk}W_{ijk} + J_{i-1jk}W_{i-1jk}}{\Delta\xi^2} +$$
$$\beta_{ijk}\frac{J_{ij+1k}W_{ij+1k} - 2J_{ijk}W_{ijk} + J_{ij-1k}W_{ij-1k}}{\Delta\eta^2} +$$
$$\gamma_{ijk}\frac{J_{ijk+1}W_{ijk+1} - 2J_{ijk}W_{ijk} + J_{ijk-1}W_{ijk-1}}{\Delta\zeta^2}\}$$
$$+\lambda_{3_{i,j,k}}\frac{P_e - P_w}{\Delta\xi} + \lambda_{2_{i,j,k}}\frac{P_n - P_s}{\Delta\eta} + S_{CONV_{ijk}}(\zeta) + S_{VIS_{ijk}}(\zeta)$$
$$-\frac{1}{Re}\{\zeta_{x_{ijk}}S_{1_{ijk}} + \zeta_{y_{ijk}}S_{2_{ijk}} + \zeta_{z_{ijk}}S_{3_{ijk}}\} = 0, \qquad (14)$$

where

$$S_{CONV_{ijk}}(\phi) = \frac{1}{\Delta\xi}\{U_e[u_e(\phi_{x_{ijk}} - \phi_{x_e}) + v_e(\phi_{y_{ijk}} - \phi_{y_e}) + w_e(\phi_{z_{ijk}} - \phi_{z_e})]$$

$$
\begin{aligned}
& -U_w[u_w(\phi_{x_{ijk}} - \phi_{x_w}) + v_w(\phi_{y_{ijk}} - \phi_{y_w}) + w_w(\phi_{z_{ijk}} - \phi_{z_w})]\} \\
+ \; & \frac{1}{\Delta\eta}\{V_n[u_n(\phi_{x_{ijk}} - \phi_{x_n}) + v_n(\phi_{y_{ijk}} - \phi_{y_n}) + w_n(\phi_{z_{ijk}} - \phi_{z_n})] \\
& -V_s[u_s(\phi_{x_{ijk}} - \phi_{x_s}) + v_s(\phi_{y_{ijk}} - \phi_{y_s}) + w_s(\phi_{z_{ijk}} - \phi_{z_s})]\} \\
+ \; & \frac{1}{\Delta\zeta}\{W_f[u_f(\phi_{x_{ijk}} - \phi_{x_f}) + v_f(\phi_{y_{ijk}} - \phi_{y_f}) + w_f(\phi_{z_{ijk}} - \phi_{z_f})] \\
& -W_b[u_b(\phi_{x_{ijk}} - \phi_{x_b}) + v_b(\phi_{y_{ijk}} - \phi_{y_b}) + w_b(\phi_{z_{ijk}} - \phi_{z_b})]\}, \qquad (15)
\end{aligned}
$$

$$
\begin{aligned}
S_{VIS_{ijk}}(\phi) \; = \; & -\frac{1}{Re}\{\frac{\alpha_{ijk}}{\Delta\xi^2}[u_{i+1jk}(\phi_{x_{ijk}} - \phi_{x_{i+1jk}}) + u_{i-1jk}(\phi_{x_{ijk}} - \phi_{x_{i-1jk}}) + \\
& v_{i+1jk}(\phi_{y_{ijk}} - \phi_{y_{i+1jk}}) + v_{i-1jk}(\phi_{y_{ijk}} - \phi_{y_{i-1jk}}) + \\
& w_{i+1jk}(\phi_{z_{ijk}} - \phi_{z_{i+1jk}}) + w_{i-1jk}(\phi_{z_{ijk}} - \phi_{z_{i-1jk}})] \\
+ \; & \frac{\beta_{ijk}}{\Delta\eta^2}[u_{ij+1k}(\phi_{x_{ijk}} - \phi_{x_{ij+1k}}) + u_{ij-1k}(\phi_{x_{ijk}} - \phi_{x_{ij-1k}}) + \\
& v_{ij+1k}(\phi_{y_{ijk}} - \phi_{y_{ij+1k}}) + v_{ij-1k}(\phi_{y_{ijk}} - \phi_{y_{ij-1k}}) + \\
& w_{ij+1k}(\phi_{z_{ijk}} - \phi_{z_{ij+1k}}) + w_{ij-1k}(\phi_{z_{ijk}} - \phi_{z_{ij-1k}})] \\
+ \; & \frac{\gamma_{ijk}}{\Delta\zeta^2}[u_{ijk+1}(\phi_{x_{ijk}} - \phi_{x_{ijk+1}}) + u_{ijk-1}(\phi_{x_{ijk}} - \phi_{x_{ijk-1}}) + \\
& v_{ijk+1}(\phi_{y_{ijk}} - \phi_{y_{ijk+1}}) + v_{ijk-1}(\phi_{y_{ijk}} - \phi_{y_{ijk-1}}) + \\
& w_{ijk+1}(\phi_{z_{ijk}} - \phi_{z_{ijk+1}}) + w_{ijk-1}(\phi_{z_{ijk}} - \phi_{z_{ijk-1}})]\}. \qquad (16)
\end{aligned}
$$

2.2 Perturbation form

The fourth-order central difference formulation for the perturbation flow can be derived as follows. Using

$$
\begin{aligned}
& \frac{1}{J}\frac{\partial u}{\partial t} + \frac{\partial[(U+U_b)u + u_bU]}{\partial\xi} + \frac{\partial[(V+V_b)u + u_bV]}{\partial\eta} + \frac{\partial[(W+W_b)u + u_bW]}{\partial\zeta} \\
& \qquad + \frac{1}{J}(\xi_x\frac{\partial}{\partial\xi} + \eta_x\frac{\partial}{\partial\eta} + \zeta_x\frac{\partial}{\partial\zeta})P - \frac{1}{JRe}\Delta_1 u \; = \; 0, \qquad (17) \\
& \frac{1}{J}\frac{\partial v}{\partial t} + \frac{\partial[(U+U_b)v + v_bU]}{\partial\xi} + \frac{\partial[(V+V_b)v + v_bV]}{\partial\eta} + \frac{\partial[(W+W_b)v + v_bW]}{\partial\zeta} \\
& \qquad + \frac{1}{J}(\xi_y\frac{\partial}{\partial\xi} + \eta_y\frac{\partial}{\partial\eta} + \zeta_y\frac{\partial}{\partial\zeta})P - \frac{1}{JRe}\Delta_1 v \; = \; 0, \qquad (18) \\
& \frac{1}{J}\frac{\partial w}{\partial t} + \frac{\partial[(U+U_b)w + w_bU]}{\partial\xi} + \frac{\partial[(V+V_b)w + w_bV]}{\partial\eta} + \frac{\partial[(W+W_b)w + w_bW]}{\partial\zeta} \\
& \qquad + \frac{1}{J}(\xi_z\frac{\partial}{\partial\xi} + \eta_z\frac{\partial}{\partial\eta} + \zeta_z\frac{\partial}{\partial\zeta})P - \frac{1}{JRe}\Delta_1 w \; = \; 0, \qquad (19)
\end{aligned}
$$

where $(u_b,\ v_b,\ w_b)$ and $(U_b,\ V_b,\ W_b)$ are base flow velocity components and their associated contravariant velocity components, we have

$$
(\frac{1}{J}\frac{\partial u}{\partial t})_{ijk} + \frac{1}{12\Delta\xi}[-(U_{i+2jk} + U_{b_{i+2jk}})u_{i+2jk} + 8(U_{i+1jk} + U_{b_{i+1jk}})u_{i+1jk}
$$

$$-8(U_{i-1jk}+U_{b_{i-1jk}})u_{i-1jk}+(U_{i-2jk}+U_{b_{i-2jk}})u_{i-2jk}]+$$

$$\frac{1}{12\Delta\eta}[-(V_{ij+2k}+V_{b_{ij+2k}})u_{ij+2k}+8(V_{ij+1k}+V_{b_{ij+1k}})u_{ij+1k}$$

$$-8(V_{ij-1k}+V_{b_{ij-1k}})u_{ij-1k}+(V_{ij-2k}+V_{b_{ij-2k}})u_{ij-2k}]+$$

$$\frac{1}{12\Delta\zeta}[-(W_{ijk+2}+W_{b_{ijk+2}})u_{ijk+2}+8(W_{ijk+1}+W_{b_{ijk+1}})u_{ijk+1}$$

$$-8(W_{ijk-1}+W_{b_{ijk-1}})u_{ijk-1}+(W_{ijk-2}+W_{b_{ijk-2}})u_{ijk-2}]+$$

$$\frac{-U_{i+2jk}u_{b_{i+2jk}}+8U_{i+1jk}u_{b_{i+1jk}}-8U_{i-1jk}u_{b_{i-1jk}}+U_{i-2jk}u_{b_{i-2jk}}}{12\Delta\xi}+$$

$$\frac{-V_{ij+2k}u_{b_{ij+2k}}+8V_{ij+1k}u_{b_{ij+1k}}-8V_{ij-1k}u_{b_{ij-1k}}+V_{ij-2k}u_{b_{ij-2k}}}{12\Delta\eta}+$$

$$\frac{-W_{ijk+2}u_{b_{ijk+2}}+8W_{ijk+1}u_{b_{ijk+1}}-8W_{ijk-1}u_{b_{ijk-1}}+W_{ijk-2}u_{b_{ijk-2}}}{12\Delta\zeta}+$$

$$\{\frac{1}{J}(\xi_x\frac{\partial}{\partial\xi}+\eta_x\frac{\partial}{\partial\eta}+\zeta_x\frac{\partial}{\partial\zeta})P\}_{ijk}-(\frac{1}{J}\frac{1}{Re}\Delta_1 u)_{ijk} = 0, \quad (20)$$

$$(\frac{1}{J}\frac{\partial v}{\partial t})_{ijk}+\frac{1}{12\Delta\xi}[-(U_{i+2jk}+U_{b_{i+2jk}})v_{i+2jk}+8(U_{i+1jk}+U_{b_{i+1jk}})v_{i+1jk}$$

$$-8(U_{i-1jk}+U_{b_{i-1jk}})v_{i-1jk}+(U_{i-2jk}+U_{b_{i-2jk}})v_{i-2jk}]+$$

$$\frac{1}{12\Delta\eta}[-(V_{ij+2k}+V_{b_{ij+2k}})v_{ij+2k}+8(V_{ij+1k}+V_{b_{ij+1k}})v_{ij+1k}$$

$$-8(V_{ij-1k}+V_{b_{ij-1k}})v_{ij-1k}+(V_{ij-2k}+V_{b_{ij-2k}})v_{ij-2k}]+$$

$$\frac{1}{12\Delta\zeta}[-(W_{ijk+2}+W_{b_{ijk+2}})v_{ijk+2}+8(W_{ijk+1}+W_{b_{ijk+1}})v_{ijk+1}$$

$$-8(W_{ijk-1}+W_{b_{ijk-1}})v_{ijk-1}+(W_{ijk-2}+W_{b_{ijk-2}})v_{ijk-2}]+$$

$$\frac{-U_{i+2jk}v_{b_{i+2jk}}+8U_{i+1jk}v_{b_{i+1jk}}-8U_{i-1jk}v_{b_{i-1jk}}+U_{i-2jk}v_{b_{i-2jk}}}{12\Delta\xi}+$$

$$\frac{-V_{ij+2k}v_{b_{ij+2k}}+8V_{ij+1k}v_{b_{ij+1k}}-8V_{ij-1k}v_{b_{ij-1k}}+V_{ij-2k}v_{b_{ij-2k}}}{12\Delta\eta}+$$

$$\frac{-W_{ijk+2}v_{b_{ijk+2}}+8W_{ijk+1}v_{b_{ijk+1}}-8W_{ijk-1}v_{b_{ijk-1}}+W_{ijk-2}v_{b_{ijk-2}}}{12\Delta\zeta}+$$

$$\{\frac{1}{J}(\xi_y\frac{\partial}{\partial\xi}+\eta_y\frac{\partial}{\partial\eta}+\zeta_y\frac{\partial}{\partial\zeta})P\}_{ijk}-(\frac{1}{J}\frac{1}{Re}\Delta_1 v)_{ijk} = 0, \quad (21)$$

$$(\frac{1}{J}\frac{\partial w}{\partial t})_{ijk}+\frac{1}{12\Delta\xi}[-(U_{i+2jk}+U_{b_{i+2jk}})w_{i+2jk}+8(U_{i+1jk}+U_{b_{i+1jk}})w_{i+1jk}$$

$$-8(U_{i-1jk}+U_{b_{i-1jk}})w_{i-1jk}+(U_{i-2jk}+U_{b_{i-2jk}})w_{i-2jk}]+$$

$$\frac{1}{12\Delta\eta}[-(V_{ij+2k}+V_{b_{ij+2k}})w_{ij+2k}+8(V_{ij+1k}+V_{b_{ij+1k}})w_{ij+1k}$$

$$-8(V_{ij-1k}+V_{b_{ij-1k}})w_{ij-1k}+(V_{ij-2k}+V_{b_{ij-2k}})w_{ij-2k}]+$$

$$\frac{1}{12\Delta\zeta}[-(W_{ijk+2}+W_{b_{ijk+2}})w_{ijk+2}+8(W_{ijk+1}+W_{b_{ijk+1}})w_{ijk+1}$$

$$-8(W_{ijk-1}+W_{b_{ijk-1}})w_{ijk-1}+(W_{ijk-2}+W_{b_{ijk-2}})w_{ijk-2}]+$$

$$\frac{-U_{i+2jk}w_{b_{i+2jk}}+8U_{i+1jk}w_{b_{i+1jk}}-8U_{i-1jk}w_{b_{i-1jk}}+U_{i-2jk}w_{b_{i-2jk}}}{12\Delta\xi}+$$

$$\frac{-V_{ij+2k}w_{b_{ij+2k}} + 8V_{ij+1k}w_{b_{ij+1k}} - 8V_{ij-1k}w_{b_{ij-1k}} + V_{ij-2k}w_{b_{ij-2k}}}{12\Delta\eta} +$$
$$\frac{-W_{ijk+2}w_{b_{ijk+2}} + 8W_{ijk+1}w_{b_{ijk+1}} - 8W_{ijk-1}w_{b_{ijk-1}} + W_{ijk-2}w_{b_{ijk-2}}}{12\Delta\zeta} +$$
$$\{\frac{1}{J}(\xi_z\frac{\partial}{\partial\xi} + \eta_z\frac{\partial}{\partial\eta} + \zeta_z\frac{\partial}{\partial\zeta})P\}_{ijk} - (\frac{1}{J}\frac{1}{Re}\Delta_1 w)_{ijk} = 0. \quad (22)$$

Do the same way as last subsection, we obtain

$$\frac{3U_{ijk} - 4U^n_{ijk} + U^{n-1}_{ijk}}{2\Delta t} +$$
$$\frac{1}{12\Delta\xi}[-J_{i+2jk}(U_{i+2jk} + U_{b_{i+2jk}})U_{i+2jk} + 8J_{i+1jk}(U_{i+1jk} + U_{b_{i+1jk}})U_{i+1jk}$$
$$-8J_{i-1jk}(U_{i-1jk} + U_{b_{i-1jk}})U_{i-1jk} + J_{i-2jk}(U_{i-2jk} + U_{b_{i-2jk}})U_{i-2jk}]$$
$$\frac{1}{12\Delta\eta}[-J_{ij+2k}(V_{ij+2k} + V_{b_{ij+2k}})U_{ij+2k} + 8J_{ij+1k}(V_{ij+1k} + V_{b_{ij+1k}})U_{ij+1k}$$
$$-8J_{ij-1k}(V_{ij-1k} + V_{b_{ij-1k}})U_{ij-1k} + J_{ij-2k}(V_{ij-2k} + V_{b_{ij-2k}})U_{ij-2k}]$$
$$\frac{1}{12\Delta\zeta}[-J_{ijk+2}(W_{ijk+2} + W_{b_{ijk+2}})U_{ijk+2} + 8J_{ijk+1}(W_{ijk+1} + W_{b_{ijk+1}})U_{ijk+1}$$
$$-8J_{ijk-1}(W_{ijk-1} + W_{b_{ijk-1}})U_{ijk-1} + J_{ijk-2}(W_{ijk-2} + W_{b_{ijk-2}})U_{ijk-2}]$$
$$+\alpha_{ijk}\frac{-P_{i+\frac{3}{2}jk} + 27P_{i+\frac{1}{2}jk} - 27P_{i-\frac{1}{2}jk} + P_{i-\frac{3}{2}jk}}{24\Delta\xi}$$
$$-\frac{1}{Re}\{\alpha_{ijk}\frac{-J_{i+2jk}U_{i+2jk} + 16J_{i+1jk}U_{i+1jk} - 30J_{ijk}U_{ijk} + 16J_{i-1jk}U_{i-1jk} - J_{i-2jk}U_{i-2jk}}{12\Delta\xi^2}$$
$$+\beta_{ijk}\frac{-J_{ij+2k}U_{ij+2k} + 16J_{ij+1k}U_{ij+1k} - 30J_{ijk}U_{ijk} + 16J_{ij-1k}U_{ij-1k} - J_{ij-2k}U_{ij-2k}}{12\Delta\eta^2}$$
$$+\gamma_{ijk}\frac{-J_{ijk+2}U_{ijk+2} + 16J_{ijk+1}U_{ijk+1} - 30J_{ijk}U_{ijk} + 16J_{ijk-1}U_{ijk-1} - J_{ijk-2}U_{ijk-2}}{12\Delta\zeta^2}\}$$
$$+S_{CONV_{ijk}}(\xi) + S_{VIS_{ijk}}(\xi) + \lambda_{1_{ijk}}\frac{P_n - P_s}{\Delta\eta} + \lambda_{3_{ijk}}\frac{P_f - P_b}{\Delta\zeta}$$
$$-\frac{1}{Re}\{\xi_{x_{ijk}}S_{1_{ijk}} + \xi_{y_{ijk}}S_{2_{ijk}} + \xi_{z_{ijk}}S_{3_{ijk}}\} = 0\ , \quad (23)$$
$$\frac{3V_{ijk} - 4V^n_{ijk} + V^{n-1}_{ijk}}{2\Delta t} +$$
$$\frac{1}{12\Delta\xi}[-J_{i+2jk}(U_{i+2jk} + U_{b_{i+2jk}})V_{i+2jk} + 8J_{i+1jk}(U_{i+1jk} + U_{b_{i+1jk}})V_{i+1jk}$$
$$-8J_{i-1jk}(U_{i-1jk} + U_{b_{i-1jk}})V_{i-1jk} + J_{i-2jk}(U_{i-2jk} + U_{b_{i-2jk}})V_{i-2jk}]$$
$$\frac{1}{12\Delta\eta}[-J_{ij+2k}(V_{ij+2k} + V_{b_{ij+2k}})V_{ij+2k} + 8J_{ij+1k}(V_{ij+1k} + V_{b_{ij+1k}})V_{ij+1k}$$
$$-8J_{ij-1k}(V_{ij-1k} + V_{b_{ij-1k}})V_{ij-1k} + J_{ij-2k}(V_{ij-2k} + V_{b_{ij-2k}})V_{ij-2k}]$$
$$\frac{1}{12\Delta\zeta}[-J_{ijk+2}(W_{ijk+2} + W_{b_{ijk+2}})V_{ijk+2} + 8J_{ijk+1}(W_{ijk+1} + W_{b_{ijk+1}})V_{ijk+1}$$
$$-8J_{ijk-1}(W_{ijk-1} + W_{b_{ijk-1}})V_{ijk-1} + J_{ijk-2}(W_{ijk-2} + W_{b_{ijk-2}})V_{ijk-2}]$$
$$+\beta_{ijk}\frac{-P_{ij+\frac{3}{2}k} + 27P_{ij+\frac{1}{2}k} - 27P_{ij-\frac{1}{2}k} + P_{ij-\frac{3}{2}k}}{24\Delta\eta}$$

$$-\frac{1}{Re}\{\alpha_{ijk}\frac{-J_{i+2jk}V_{i+2jk}+16J_{i+1jk}V_{i+1jk}-30J_{ijk}V_{ijk}+16J_{i-1jk}V_{i-1jk}-J_{i-2jk}V_{i-2jk}}{12\Delta\xi^2}$$
$$+\beta_{ijk}\frac{-J_{ij+2k}V_{ij+2k}+16J_{ij+1k}V_{ij+1k}-30J_{ijk}V_{ijk}+16J_{ij-1k}V_{ij-1k}-J_{ij-2k}V_{ij-2k}}{12\Delta\eta^2}$$
$$+\gamma_{ijk}\frac{-J_{ijk+2}V_{ijk+2}+16J_{ijk+1}V_{ijk+1}-30J_{ijk}V_{ijk}+16J_{ijk-1}V_{ijk-1}-J_{ijk-2}V_{ijk-2}}{\Delta\zeta^2}\}$$
$$+\lambda_{1_{ijk}}\frac{P_e-P_w}{\Delta\xi}+\lambda_{2_{ijk}}\frac{P_f-P_b}{\Delta\zeta}+S_{CONV_{ijk}}(\eta)+S_{VIS_{ijk}}(\eta)$$
$$-\frac{1}{Re}\{\eta_{x_{ijk}}S_{1_{ijk}}+\eta_{y_{ijk}}S_{2_{ijk}}+\eta_{z_{ijk}}S_{3_{ijk}}\}=0\ , \quad (24)$$
$$\frac{3W_{ijk}-4W^n_{ijk}+W^{n-1}_{ijk}}{12\Delta t}+$$
$$\frac{1}{12\Delta\xi}[-J_{i+2jk}(U_{i+2jk}+U_{b_{i+2jk}})W_{i+2jk}+8J_{i+1jk}(U_{i+1jk}+U_{b_{i+1jk}})W_{i+1jk}$$
$$-8J_{i-1jk}(U_{i-1jk}+U_{b_{i-1jk}})W_{i-1jk}+J_{i-2jk}(U_{i-2jk}+U_{b_{i-2jk}})W_{i-2jk}]$$
$$\frac{1}{12\Delta\eta}[-J_{ij+2k}(V_{ij+2k}+V_{b_{ij+2k}})W_{ij+2k}+8J_{ij+1k}(V_{ij+1k}+V_{b_{ij+1k}})W_{ij+1k}$$
$$-8J_{ij-1k}(V_{ij-1k}+V_{b_{ij-1k}})W_{ij-1k}+J_{ij-2k}(V_{ij-2k}+V_{b_{ij-2k}})W_{ij-2k}]$$
$$\frac{1}{12\Delta\zeta}[-J_{ijk+2}(W_{ijk+2}+W_{b_{ijk+2}})W_{ijk+2}+8J_{ijk+1}(W_{ijk+1}+W_{b_{ijk+1}})W_{ijk+1}$$
$$-8J_{ijk-1}(W_{ijk-1}+W_{b_{ijk-1}})W_{ijk-1}+J_{ijk-2}(W_{ijk-2}+W_{b_{ijk-2}})W_{ijk-2}]$$
$$+\gamma_{ijk}\frac{-P_{ijk+\frac{3}{2}}+27P_{ijk+\frac{1}{2}}-27P_{ijk-\frac{1}{2}}+P_{ijk-\frac{3}{2}}}{24\Delta\zeta}$$
$$-\frac{1}{Re}\{\alpha_{ijk}\frac{-J_{i+2jk}W_{i+2jk}+16J_{i+1jk}W_{i+1jk}-30J_{ijk}W_{ijk}+16J_{i-1jk}W_{i-1jk}-J_{i-2jk}W_{i-2jk}}{12\Delta\xi^2}$$
$$+\beta_{ijk}\frac{-J_{ij+2k}W_{ij+2k}+16J_{ij+1k}W_{ij+1k}-30J_{ijk}W_{ijk}+16J_{ij-1k}W_{ij-1k}-J_{ij-2k}W_{ij-2k}}{12\Delta\eta^2}$$
$$+\gamma_{ijk}\frac{-J_{ijk+2}W_{ijk+2}+16J_{ijk+1}W_{ijk+1}-30J_{ijk}W_{ijk}+16J_{ijk-1}W_{ijk-1}-J_{ijk-2}W_{ijk-2}}{12\Delta\zeta^2}\}$$
$$\lambda_3\frac{P_e-P_w}{\Delta\xi}+\lambda_2\frac{P_n-P_s}{\Delta\eta}+S_{CONV_{ijk}}(\zeta)+S_{VIS_{ijk}}(\zeta)$$
$$-\frac{1}{Re}\{\zeta_{x_{ijk}}S_{1_{ijk}}+\zeta_{y_{ijk}}S_{2_{ijk}}+\zeta_{z_{ijk}}S_{3_{ijk}}\}=0\ , \quad (25)$$

where

$$\begin{aligned}S_{CONV_{ijk}}(\phi) \;=\; & \frac{1}{12\Delta\xi}\{-(U_{i+2jk}+U_{b_{i+2jk}})[u_{i+2jk}(\phi_{x_{ijk}}-\phi_{x_{i+2jk}})\\ & +v_{i+2jk}(\phi_{y_{ijk}}-\phi_{y_{i+2jk}})+w_{i+2jk}(\phi_{z_{ijk}}-\phi_{z_{i+2jk}})]\\ & +8(U_{i+1jk}+U_{b_{i+1jk}})[u_{i+1jk}(\phi_{x_{ijk}}-\phi_{x_{i+1jk}})\\ & +v_{i+1jk}(\phi_{y_{ijk}}-\phi_{y_{i+1jk}})+w_{i+1jk}(\phi_{z_{ijk}}-\phi_{z_{i+1jk}})]\\ & -8(U_{i-1jk}+U_{b_{i-1jk}})[u_{i-1jk}(\phi_{x_{ijk}}-\phi_{x_{i-1jk}})\\ & +v_{i-1jk}(\phi_{y_{ijk}}-\phi_{y_{i-1jk}})+w_{i-1jk}(\phi_{z_{ijk}}-\phi_{z_{i-1jk}})]\end{aligned}$$

$$
\begin{aligned}
&+(U_{i-2jk}+U_{b_{i-2jk}})[u_{i-2jk}(\phi_{x_{ijk}}-\phi_{x_{i-2jk}})\\
&+v_{i-2jk}(\phi_{y_{ijk}}-\phi_{y_{i-2jk}})+w_{i-2jk}(\phi_{z_{ijk}}-\phi_{z_{i-2jk}})]\}\\
+\ &\frac{1}{12\Delta\eta}\{-(V_{ij+2k}+V_{b_{ij+2k}})[u_{ij+2k}(\phi_{x_{ijk}}-\phi_{x_{ij+2k}})\\
&+v_{ij+2k}(\phi_{y_{ijk}}-\phi_{y_{ij+2k}})+w_{ij+2k}(\phi_{z_{ijk}}-\phi_{z_{ij+2k}})]\\
&+8(V_{ij+1k}+V_{b_{ij+1k}})[u_{ij+1k}(\phi_{x_{ijk}}-\phi_{x_{ij+1k}})\\
&+v_{ij+1k}(\phi_{y_{ijk}}-\phi_{y_{ij+1k}})+w_{ij+1k}(\phi_{z_{ijk}}-\phi_{z_{ij+1k}})]\\
&-8(V_{ij-1k}+V_{b_{ij-1k}})[u_{ij-1k}(\phi_{x_{ijk}}-\phi_{x_{ij-1k}})\\
&+v_{ij-1k}(\phi_{y_{ijk}}-\phi_{y_{ij-1k}})+w_{ij-1k}(\phi_{z_{ijk}}-\phi_{z_{ij-1k}})]\\
&+(V_{ij-2k}+V_{b_{ij-2k}})[u_{ij-2k}(\phi_{x_{ijk}}-\phi_{x_{ij-2k}})\\
&+v_{ij-2k}(\phi_{y_{ijk}}-\phi_{y_{ij-2k}})+w_{ij-2k}(\phi_{z_{ijk}}-\phi_{z_{ij-2k}})]\}\\
+\ &\frac{1}{12\Delta\zeta}\{-(W_{ijk+2}+W_{b_{ijk+2}})[u_{ijk+2}(\phi_{x_{ijk}}-\phi_{x_{ijk+2}})\\
&+v_{ijk+2}(\phi_{y_{ijk}}-\phi_{y_{ijk+2}})+w_{ijk+2}(\phi_{z_{ijk}}-\phi_{z_{ijk+2}})]\\
&+8(W_{ijk+1}+W_{b_{ijk+1}})[u_{ijk+1}(\phi_{x_{ijk}}-\phi_{x_{ijk+1}})\\
&+v_{ijk+1}(\phi_{y_{ijk}}-\phi_{y_{ijk+1}})+w_{ijk+1}(\phi_{z_{ijk}}-\phi_{z_{ijk+1}})]\\
&-8(W_{ijk-1}+W_{b_{ijk-1}})[u_{ijk-1}(\phi_{x_{ijk}}-\phi_{x_{ijk-1}})\\
&+v_{ijk-1}(\phi_{y_{ijk}}-\phi_{y_{ijk-1}})+w_{ijk-1}(\phi_{z_{ijk}}-\phi_{z_{ijk-1}})]\\
&+(W_{ijk-2}+W_{b_{ijk-2}})[u_{ijk-2}(\phi_{x_{ijk}}-\phi_{x_{ijk-2}})\\
&+v_{ijk-2}(\phi_{y_{ijk}}-\phi_{y_{ijk-2}})+w_{ijk-2}(\phi_{z_{ijk}}-\phi_{z_{ijk-2}})]\}\\
+\ &\frac{1}{12\Delta\xi}\{-U_{i+2jk}(u_{b_{i+2jk}}\phi_{x_{ijk}}+v_{b_{i+2jk}}\phi_{y_{ijk}}+w_{b_{i+2jk}}\phi_{z_{ijk}})\\
&+8U_{i+1jk}(u_{b_{i+1jk}}\phi_{x_{ijk}}+v_{b_{i+1jk}}\phi_{y_{ijk}}+w_{b_{i+1jk}}\phi_{z_{ijk}})\\
&-8U_{i-1jk}(u_{b_{i-1jk}}\phi_{x_{ijk}}+v_{b_{i-1jk}}\phi_{y_{ijk}}+w_{b_{i-1jk}}\phi_{z_{ijk}})\\
&+U_{i-2jk}(u_{b_{i-2jk}}\phi_{x_{ijk}}+v_{b_{i-2jk}}\phi_{y_{ijk}}+w_{b_{i-2jk}}\phi_{z_{ijk}})\}\\
+\ &\frac{1}{12\Delta\eta}\{-V_{ij+2k}(u_{b_{ij+2k}}\phi_{x_{ijk}}+v_{b_{ij+2k}}\phi_{y_{ijk}}+w_{b_{ij+2k}}\phi_{z_{ijk}})\\
&+8V_{ij+1k}(u_{b_{ij+1k}}\phi_{x_{ijk}}+v_{b_{ij+1k}}\phi_{y_{ijk}}+w_{b_{ij+1k}}\phi_{z_{ijk}})\\
&-8V_{ij-1k}(u_{b_{ij-1k}}\phi_{x_{ijk}}+v_{b_{ij-1k}}\phi_{y_{ijk}}+w_{b_{ij-1k}}\phi_{z_{ijk}})\\
&+V_{ij-2k}(u_{b_{ij-2k}}\phi_{x_{ijk}}+v_{b_{ij-2k}}\phi_{y_{ijk}}+w_{b_{ij-2k}}\phi_{z_{ijk}})\}\\
+\ &\frac{1}{12\Delta\zeta}\{-W_{ijk+2}(u_{b_{ijk+2}}\phi_{x_{ijk}}+v_{b_{ijk+2}}\phi_{y_{ijk}}+w_{b_{ijk+2}}\phi_{z_{ijk}})\\
&+8W_{ijk+1}(u_{b_{ijk+1}}\phi_{x_{ijk}}+v_{b_{ijk+1}}\phi_{y_{ijk}}+w_{b_{ijk+1}}\phi_{z_{ijk}})
\end{aligned}
$$

$$
\begin{aligned}
& -8W_{ijk-1}(u_{b_{ijk-1}}\phi_{x_{ijk}} + v_{b_{ijk-1}}\phi_{y_{ijk}} + w_{b_{ijk-1}}\phi_{z_{ijk}}) \\
& +W_{ijk-2}(u_{b_{ijk-2}}\phi_{x_{ijk}} + v_{b_{ijk-2}}\phi_{y_{ijk}} + w_{b_{ijk-2}}\phi_{z_{ijk}})\}, \qquad (26)
\end{aligned}
$$

$$
\begin{aligned}
S_{VIS_{ijk}}(\phi) \;=\; & -\frac{1}{Re}\{\frac{\alpha_{ijk}}{12\Delta\xi^2}[-u_{i+2jk}(\phi_{x_{ijk}} - \phi_{x_{i+2jk}}) + 16u_{i+1jk}(\phi_{x_{ijk}} - \phi_{x_{i+1jk}}) \\
& +16u_{i-1jk}(\phi_{x_{ijk}} - \phi_{x_{i-1jk}}) - u_{i-2jk}(\phi_{x_{ijk}} - \phi_{x_{i-2jk}}) \\
& -v_{i+2jk}(\phi_{y_{ijk}} - \phi_{y_{i+2jk}}) + 16v_{i+1jk}(\phi_{y_{ijk}} - \phi_{y_{i+1jk}}) \\
& +16v_{i-1jk}(\phi_{y_{ijk}} - \phi_{y_{i-1jk}}) - v_{i-2jk}(\phi_{y_{ijk}} - \phi_{y_{i-2jk}}) \\
& -w_{i+2jk}(\phi_{z_{ijk}} - \phi_{z_{i+2jk}}) + 16w_{i+1jk}(\phi_{z_{ijk}} - \phi_{z_{i+1jk}}) \\
& +16w_{i-1jk}(\phi_{z_{ijk}} - \phi_{z_{i-1jk}}) - w_{i-2jk}(\phi_{z_{ijk}} - \phi_{z_{i-2jk}})] \\
& + \frac{\beta_{ijk}}{12\Delta\eta^2}[-u_{ij+2k}(\phi_{x_{ijk}} - \phi_{x_{ij+2k}}) + 16u_{ij+1k}(\phi_{x_{ijk}} - \phi_{x_{ij+1k}}) \\
& +16u_{ij-1k}(\phi_{x_{ijk}} - \phi_{x_{ij-1k}}) - u_{ij-2k}(\phi_{x_{ijk}} - \phi_{x_{ij-2k}}) \\
& -v_{ij+2k}(\phi_{y_{ijk}} - \phi_{y_{ij+2k}}) + 16v_{ij+1k}(\phi_{y_{ijk}} - \phi_{y_{ij+1k}}) \\
& +16v_{ij-1k}(\phi_{y_{ijk}} - \phi_{y_{ij-1k}}) - v_{ij-2k}(\phi_{y_{ijk}} - \phi_{y_{ij-2k}}) \\
& -w_{ij+2k}(\phi_{z_{ijk}} - \phi_{z_{ij+2k}}) + 16w_{ij+1k}(\phi_{z_{ijk}} - \phi_{z_{ij+1k}}) \\
& +16w_{ij-1k}(\phi_{z_{ijk}} - \phi_{z_{ij-1k}}) - w_{ij-2k}(\phi_{z_{ijk}} - \phi_{z_{ij-2k}})] \\
& + \frac{\gamma_{ijk}}{12\Delta\zeta^2}[-u_{ijk+2}(\phi_{x_{ijk}} - \phi_{x_{ijk+2}}) + 16u_{ijk+1}(\phi_{x_{ijk}} - \phi_{x_{ijk+1}}) \\
& +16u_{ijk-1}(\phi_{x_{ijk}} - \phi_{x_{ijk-1}}) - u_{ijk-2}(\phi_{x_{ijk}} - \phi_{x_{ijk-2}}) \\
& -v_{ijk+2}(\phi_{y_{ijk}} - \phi_{y_{ijk+2}}) + 16v_{ijk+1}(\phi_{y_{ijk}} - \phi_{y_{ijk+1}}) \\
& +16v_{ijk-1}(\phi_{y_{ijk}} - \phi_{y_{ijk-1}}) - v_{ijk-2}(\phi_{y_{ijk}} - \phi_{y_{ijk-2}}) \\
& -w_{ijk+2}(\phi_{z_{ijk}} - \phi_{z_{ijk+2}}) + 16w_{ijk+1}(\phi_{z_{ijk}} - \phi_{z_{ijk+1}}) \\
& +16w_{ijk-1}(\phi_{z_{ijk}} - \phi_{z_{ijk-1}}) - w_{ijk-1}(\phi_{z_{ijk}} - \phi_{z_{ijk-1}})]\}. \qquad (27)
\end{aligned}
$$

3 Conformal Mapping

Since transition (especially in the receptivity regime) is very sensitive to any kind of disturbance, physical or numerical, a highly accurate scheme is required for the computational domain transformation. To assure the numerical scheme for the flow not to lose accuracy, we should make the accuracy of grid transformation schemes at least the same order as that of the flow scheme itself.

As the first step, relatively simple configurations are considered, and this enables us to use the analytical/conformal mapping to obtain the required transformation coefficients (Jacobi metrics).

For an H-type grid, the Joukowsky transformation is adopted.

3.1 Conformal mapping for a quarter of cylinder

For a quarter of cylinder, a three-step transformation is required to transfer the physical domain to the computational domain (see Figure 2):

1. $(\xi, \eta) \Rightarrow (\xi_1, \eta_1)$:

$$\begin{aligned} \xi_1 &= \frac{1}{\sigma_A}\xi, \\ \eta_1 &= \eta. \end{aligned}$$

This will ensure the points (0,0) and $(a, 0)$ in the (ξ_1, η_1) space match the points $(-a, 0)$ and $(0, a)$ in the (x, y) space.

2. $(\xi_1, \eta_1) \Rightarrow (x_1, y_1)$:

$$\begin{aligned} x_1 &= \frac{\sigma_B \xi}{\sigma_B + a - |\xi_1|} - a, \\ y_1 &= \frac{\sigma_C y_{1_{max}} \eta_1}{\sigma_C \eta_{max} + y_{1_{max}}(\eta_{max} - \eta_1)}. \end{aligned}$$

This includes stretching in both directions. The smaller the σ_B and σ_C, the stronger the stretching near the solid wall and the leading edge, respectively. The associated inverse transformation is

$$\begin{aligned} \xi_1 &= \begin{cases} \frac{(x_1+a)(\sigma_B+a)}{\sigma_B+x_1+a} & (x_1 > -a), \\ \frac{(x_1+a)(\sigma_B+a)}{\sigma_B-(x_1+a)} & (x_1 \leq -a), \end{cases} \\ \eta_1 &= \frac{\eta_{max} y_1 (\sigma_C + y_{1_{max}})}{y_{1_{max}}(\sigma_C + y_1)}. \end{aligned}$$

3. $(x_1, y_1) \Rightarrow (x, y)$: Joukowsky transformation

$$\begin{aligned} x_1 &= \frac{x}{2}(1 + \frac{a^2}{x^2 + y^2}), \\ y_1 &= \frac{y}{2}(1 - \frac{a^2}{x^2 + y^2}). \end{aligned}$$

The associated derivatives in this step are

$$\begin{aligned} x_{1_x} &= \frac{1}{2} + \frac{a^2}{2}\frac{y^2 - x^2}{(x^2 + y^2)^2}, \\ x_{1_y} &= -\frac{a^2 xy}{(x^2 + y^2)^2}, \end{aligned}$$

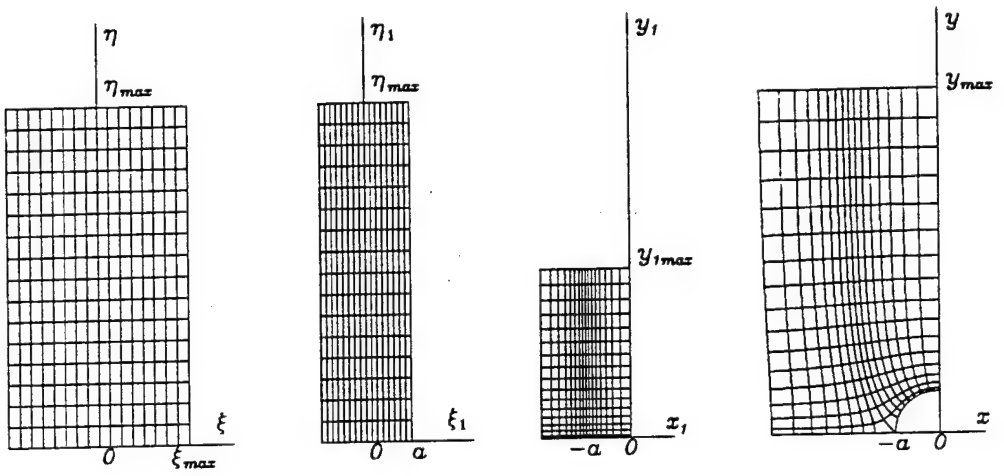

Figure 2. Transformation process for a quarter of cylinder.

$$
\begin{aligned}
x_{1_{xx}} &= \frac{a^2 x}{(x^2+y^2)^3}(x^2-3y^2), \\
x_{1_{yy}} &= -\frac{a^2 x}{(x^2+y^2)^3}(x^2-3y^2), \\
y_{1_x} &= \frac{a^2 xy}{(x^2+y^2)^2}, \\
y_{1_y} &= \frac{1}{2}+\frac{a^2}{2}\frac{y^2-x^2}{(x^2+y^2)^2}, \\
y_{1_{xx}} &= \frac{a^2 y}{(x^2+y^2)^3}(y^2-3x^2), \\
y_{1_{yy}} &= -\frac{a^2 y}{(x^2+y^2)^3}(y^2-3x^2).
\end{aligned}
$$

Thus, we have

- $x_1 > -a$:

$$
\begin{aligned}
\xi_x &= \xi_{\xi_1}\xi_{1_x} \\
&= \frac{\sigma_A\sigma_B(\sigma_B+a)}{(\sigma_B+x_1+a)^2}x_{1_x}, \\
\xi_y &= \xi_{\xi_1}\xi_{1_y} \\
&= \frac{\sigma_A\sigma_B(\sigma_B+a)}{(\sigma_B+x_1+a)^2}x_{1_y}, \\
\xi_{xx} &= \frac{\sigma_A\sigma_B(\sigma_B+a)}{(\sigma_B+x_1+a)^3}[x_{1_{xx}}(\sigma_B+x_1+a)-2x_{1_x}^2],
\end{aligned}
$$

$$\xi_{yy} = \frac{\sigma_A\sigma_B(\sigma_B+a)}{(\sigma_B+x_1+a)^3}[x_{1_{yy}}(\sigma_B+x_1+a)-2x_{1_y}^2]. \tag{28}$$

- $x_1 \le -a$:

$$\begin{aligned}
\xi_x &= \frac{\sigma_A\sigma_B(\sigma_B+a)}{(\sigma_B-(x_1+a))^2}x_{1_x},\\
\xi_y &= \frac{\sigma_A\sigma_B(\sigma_B+a)}{(\sigma_B-(x_1+a))^2}x_{1_y},\\
\xi_{xx} &= \frac{\sigma_A\sigma_B(\sigma_B+a)}{(\sigma_B-(x_1+a))^3}\{x_{1_{xx}}[\sigma_B-(x_1+a)]+2x_{1_x}^2\},\\
\xi_{yy} &= \frac{\sigma_A\sigma_B(\sigma_B+a)}{(\sigma_B-(x_1+a))^3}\{x_{1_{yy}}[\sigma_B-(x_1+a)]+2x_{1_y}^2\}.
\end{aligned} \tag{29}$$

- normal direction:

$$\begin{aligned}
\eta_x &= \frac{\eta_{max}(\sigma_C+y_{1_{max}})}{y_{1_{max}}}\frac{\sigma_C y_{1_x}}{(\sigma_C+y_1)^2},\\
\eta_y &= \frac{\eta_{max}(\sigma_C+y_{1_{max}})}{y_{1_{max}}}\frac{\sigma_C y_{1_y}}{(\sigma_C+y_1)^2},\\
\eta_{xx} &= \frac{\sigma_C\eta_{max}(\sigma_C+y_{1_{max}})}{y_{1_{max}}}y_{1_{xx}}(\sigma_C+y_{1_{max}})-2y_{1_x}^2(\sigma_C+y_1)^3,\\
\eta_{yy} &= \frac{\sigma_C\eta_{max}(\sigma_C+y_{1_{max}})}{y_{1_{max}}}y_{1_{yy}}(\sigma_C+y_{1_{max}})-2y_{1_y}^2(\sigma_C+y_1)^3.
\end{aligned} \tag{30}$$

For the geometry other than a cylinder, more transformation steps are required.

3.2 Conformal mapping for the leading-edge flat-plate juncture

The transformation process can be described as follows (see Figure 3):

1. $(\xi,\eta) \Rightarrow (\xi_0,\eta_0)$:

$$\begin{aligned}
\xi_0 &= \frac{1}{\sigma_A}\xi,\\
\eta_0 &= \eta\,.
\end{aligned}$$

2. $(\xi_0,\eta_0) \Rightarrow (\xi_1,\eta_1)$:

$$\begin{aligned}
\xi_1 &= \frac{\sigma_B\xi_0}{\sigma_B+a-|\xi_0|}-a,\\
\eta_1 &= \frac{\sigma_C\eta_{1_{max}}\eta_0}{\sigma_C\eta_{max}+\eta_{1_{max}}(\eta_{max}-\eta_0)}.
\end{aligned}$$

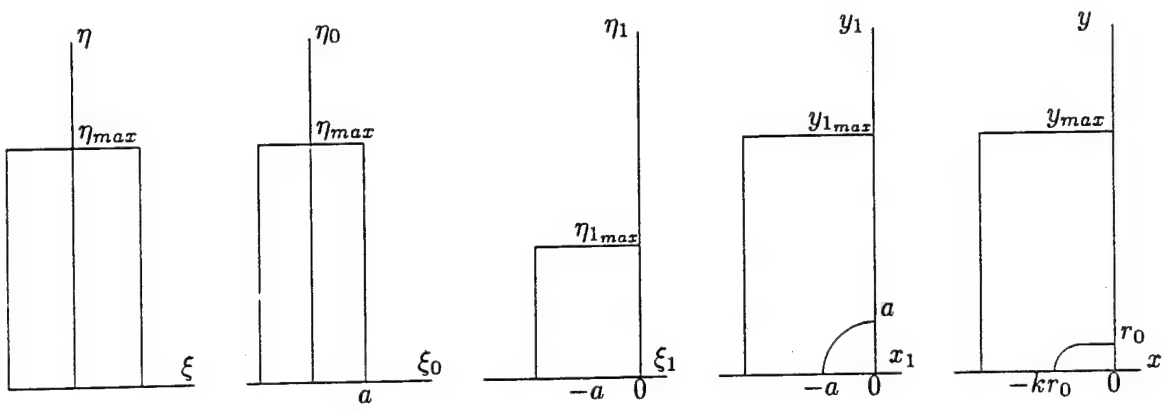

Figure 3. Transformation process for an elliptic leading-edge.

3. $(\xi_1, \eta_1) \Rightarrow (x_1, y_1)$: Joukowsky transformation

$$\begin{aligned} \xi_1 &= \frac{x_1}{2}(1 + \frac{a^2}{x_1^2 + y_1^2}), \\ \eta_1 &= \frac{y_1}{2}(1 - \frac{a^2}{x_1^2 + y_1^2}). \end{aligned}$$

4. $(x_1, y_1, z_1) \Rightarrow (x, y, z)$:

$$\begin{aligned} x &= \sigma_D x_1[1 + \frac{k^2 - 1}{(k+1)^2}\frac{1}{x_1^2 + y_1^2}], \\ y &= \sigma_D y_1[1 - \frac{k^2 - 1}{(k+1)^2}\frac{1}{x_1^2 + y_1^2}], \end{aligned}$$

where axes of the ellipse are (r_0, kr_0), with

$$a = \frac{r_0(k+1)}{2\sigma_D}.$$

3.3 Conformal mapping for Joukowsky airfoil

The transformation process for Joukowsky airfoil can be described as follows:

1. $(\xi, \eta) \Rightarrow (\xi_0, \eta_0)$:

$$\begin{aligned} \xi_0 &= \frac{1}{\sigma_A}\xi, \\ \eta_0 &= \eta\,. \end{aligned}$$

2. $(\xi_0, \eta_0) \Rightarrow (\xi_1, \eta_1)$:

$$\begin{aligned} \xi_1 &= \frac{\sigma_B \xi_0}{\sigma_B + a - |\xi_0|} - a, \\ \eta_1 &= \frac{\sigma_C \eta_{1_{max}} \eta_0}{\sigma_C \eta_{max} + \eta_{1_{max}}(\eta_{max} - \eta_0)}. \end{aligned}$$

3. $(\xi_1, \eta_1) \Rightarrow (x_1, y_1)$: Joukowsky transformation

$$\begin{aligned} \xi_1 &= \frac{x_1}{2}(1 + \frac{a^2}{x_1^2 + y_1^2}), \\ \eta_1 &= \frac{y_1}{2}(1 - \frac{a^2}{x_1^2 + y_1^2}). \end{aligned}$$

4. $(x_1, y_1) \Rightarrow (x_2, y_2)$:

$$\begin{aligned} x_2 &= x_1 - \frac{k'a}{k'+1}, \\ y_2 &= y_1. \end{aligned}$$

5. $(x_2, y_2) \rightarrow (x, y)$:

$$\begin{aligned} x &= \sigma_E x_2 (1 + \frac{a^2}{(k'+1)^2} \frac{1}{x_2^2 + y_2^2}), \\ y &= \sigma_E y_2 (1 - \frac{a^2}{(k'+1)^2} \frac{1}{x_2^2 + y_2^2}). \end{aligned}$$

Here, $k' < 1$ is used to change the ratio of half-thickness/chord-length of the airfoil. For example, with $k' = 0.0116$, the ratio=1/16. Also, we use σ_E to normalize the airfoil and make the half-thickness equal to 1 (see Figure 4).

The chain-rule is applied to obtain the required metrics. For example,

$$\begin{aligned} \xi_x &= \xi_{x_1} x_{1_x} + \xi_{y_1} y_{1_x} + \xi_{z_1} z_{1_x}, \\ \xi_y &= \xi_{x_1} x_{1_y} + \xi_{y_1} y_{1_y} + \xi_{z_1} z_{1_y}, \\ \xi_z &= \xi_{x_1} x_{1_z} + \xi_{y_1} y_{1_z} + \xi_{z_1} z_{1_z}, \\ \eta_x &= \eta_{x_1} x_{1_x} + \eta_{y_1} y_{1_x} + \eta_{z_1} z_{1_x}, \\ \eta_y &= \eta_{x_1} x_{1_y} + \eta_{y_1} y_{1_y} + \eta_{z_1} z_{1_y}, \\ \eta_z &= \eta_{x_1} x_{1_z} + \eta_{y_1} y_{1_z} + \eta_{z_1} z_{1_z}, \\ \zeta_x &= \zeta_{x_1} x_{1_x} + \zeta_{y_1} y_{1_x} + \zeta_{z_1} z_{1_x}, \\ \zeta_y &= \zeta_{x_1} x_{1_y} + \zeta_{y_1} y_{1_y} + \zeta_{z_1} z_{1_y}, \\ \zeta_z &= \zeta_{x_1} x_{1_z} + \zeta_{y_1} y_{1_z} + \zeta_{z_1} z_{1_z}, \end{aligned}$$

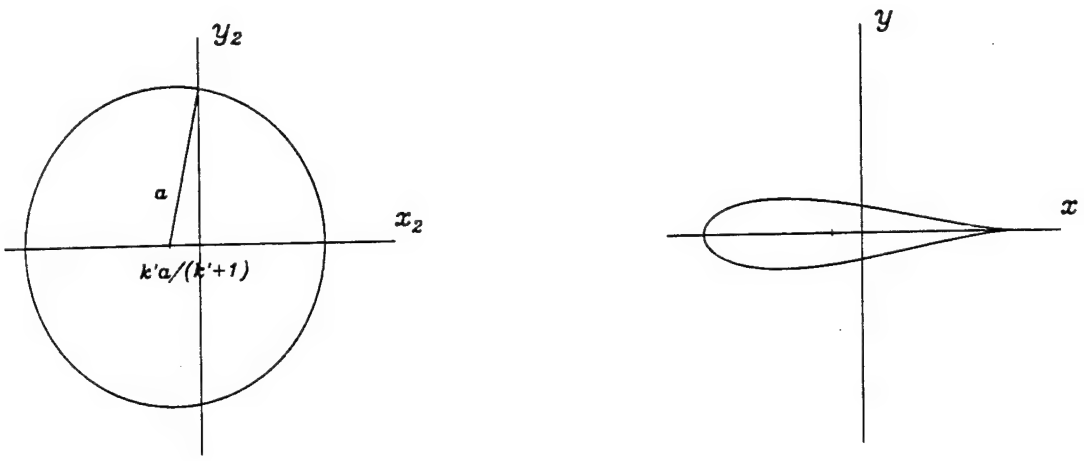

Figure 4. Transformation process for a Joukowsky airfoil.

with

$$
\begin{aligned}
\xi_{x_1} &= \xi_{\xi_1}\xi_{1x_1} + \xi_{\eta_1}\eta_{1x_1} + \xi_{\zeta_1}\zeta_{1x_1}, \\
\xi_{y_1} &= \xi_{\xi_1}\xi_{1y_1} + \xi_{\eta_1}\eta_{1y_1} + \xi_{\zeta_1}\zeta_{1y_1}, \\
\xi_{z_1} &= \xi_{\xi_1}\xi_{1z_1} + \xi_{\eta_1}\eta_{1z_1} + \xi_{\zeta_1}\zeta_{1z_1}, \\
\eta_{x_1} &= \eta_{\xi_1}\xi_{1x_1} + \eta_{\eta_1}\eta_{1x_1} + \eta_{\zeta_1}\zeta_{1x_1}, \\
\eta_{y_1} &= \eta_{\xi_1}\xi_{1y_1} + \eta_{\eta_1}\eta_{1y_1} + \eta_{\zeta_1}\zeta_{1y_1}, \\
\eta_{z_1} &= \eta_{\xi_1}\xi_{1z_1} + \eta_{\eta_1}\eta_{1z_1} + \eta_{\zeta_1}\zeta_{1z_1}, \\
\zeta_{x_1} &= \zeta_{\xi_1}\xi_{1x_1} + \zeta_{\eta_1}\eta_{1x_1} + \zeta_{\zeta_1}\zeta_{1x_1}, \\
\zeta_{y_1} &= \zeta_{\xi_1}\xi_{1y_1} + \zeta_{\eta_1}\eta_{1y_1} + \zeta_{\zeta_1}\zeta_{1y_1}, \\
\zeta_{z_1} &= \zeta_{\xi_1}\xi_{1z_1} + \zeta_{\eta_1}\eta_{1z_1} + \zeta_{\zeta_1}\zeta_{1z_1}.
\end{aligned}
$$

The second-order derivatives can be obtained through:

$$
\begin{aligned}
\xi_{xx} &= \xi_{x\xi}\xi_x + \xi_{x\eta}\eta_x + \xi_{x\zeta}\zeta_x, \\
\xi_{yy} &= \xi_{y\xi}\xi_y + \xi_{y\eta}\eta_y + \xi_{y\zeta}\zeta_y, \\
\xi_{zz} &= \xi_{z\xi}\xi_z + \xi_{z\eta}\eta_z + \xi_{z\zeta}\zeta_z, \\
\eta_{xx} &= \eta_{x\xi}\xi_x + \eta_{x\eta}\eta_x + \eta_{x\zeta}\zeta_x, \\
\eta_{yy} &= \eta_{y\xi}\xi_y + \eta_{y\eta}\eta_y + \eta_{y\zeta}\zeta_y,
\end{aligned}
$$

$$
\begin{aligned}
\eta_{zz} &= \eta_{z\xi}\xi_z + \eta_{z\eta}\eta_z + \eta_{z\zeta}\zeta_z, \\
\zeta_{xx} &= \zeta_{x\xi}\xi_x + \zeta_{x\eta}\eta_x + \zeta_{x\zeta}\zeta_x, \\
\zeta_{yy} &= \zeta_{y\xi}\xi_y + \zeta_{y\eta}\eta_y + \zeta_{y\zeta}\zeta_y, \\
\zeta_{zz} &= \zeta_{z\xi}\xi_z + \zeta_{z\eta}\eta_z + \zeta_{z\zeta}\zeta_z.
\end{aligned}
$$

4 Numerical Process

In the computational (ξ, η, ζ) space, the grids are uniform. Suppose U, V, W are defined in terms of a staggered grid in the computational space (see Figure 5). Here, the values of u, v, w, P are associated with its cell centers, U with centers of the cell surfaces parallel to the (η, ζ) plane, V with centers of the cell surfaces parallel to the (ξ, ζ) plane, and W with centers of the cell surfaces parallel to the (ξ, η) plane.

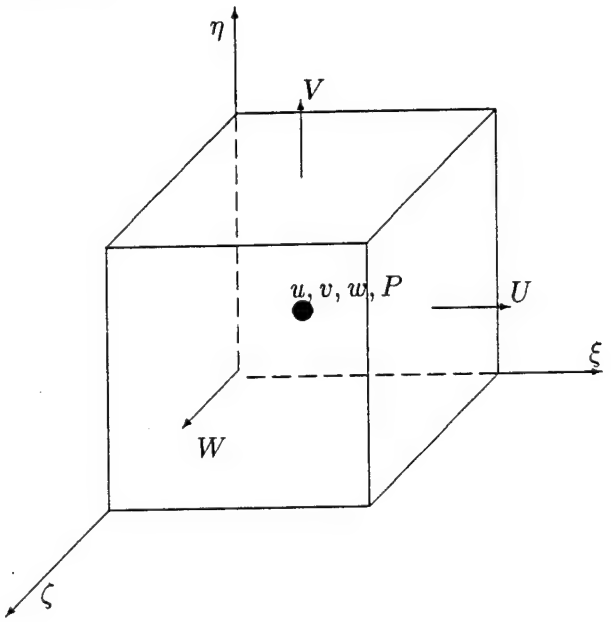

Figure 5. Staggered grid structure in the computational (ξ, η, ζ) space.

The approaches used in this work include

- Base flow
  1. Hybrid scheme in space (Patankar & Spalding, 1972)
  2. Line-distributive relaxation (Liu & Liu, 1993)

3. Multigrid FAS (Brandt, 1984)

- Perturbation flow

1. Second-order backward Euler in time
2. Fourth-order central difference in space (Liu & Liu, 1993)
3. Line-distributive relaxation (Liu & Liu, 1993)
4. Buffered-outflow boundary condition (Liu & Liu, 1993)
5. Inter-grid dissipation (Liu & Liu, 1995)

A basic state flow field is first solved. Since the H-type grid is used, we do not need large number of grid points in the wall-normal direction (C-type grid usually needs more grid points because the wall-normal direction is almost parallel to the main flow direction in some region). The perturbation system is then solved.

5 Computational Results

Based on the above formulation, a number of computer codes for grid generation, base flow, and perturbation flow have been developed.

5.1 Code validation

5.1.1 Linear stage

The validation of the code is first examined on the linear instability stage for a smooth flat plate.

The inflow perturbation for the 2D case is

$$\mathbf{u}(0,y,z,t) = \text{Real}\{\epsilon_{2d}\phi_{2d}^{(k)}(y)e^{-i\omega_{2d}t}\}, \tag{31}$$

for the 3D case is

$$\mathbf{u}(0,y,z,t) = \text{Real}\{\epsilon_{3d}\phi_{3d}^{(k)}(y)e^{-i\omega_{3d}t+i\beta z}\},. \tag{32}$$

and for the 3D nonlinear breakdown case is

$$\mathbf{u}(0,y,z,t) = \text{Real}\{\epsilon_{2d}\phi_{2d}^{(k)}(y)e^{-i\omega_{2d}t} + \epsilon_{3d}\phi_{3d}^{(k)}(y)e^{-i\omega_{3d}t+i\beta z} + \epsilon_{3d}\phi_{3d}^{(k)}(y)e^{-i\omega_{3d}t-i\beta z}\}. \tag{33}$$

Here, ϵ_{2d} and ϵ_{3d} are the amplitude of 2D and 3D disturbances. The grid transformation function in the wall-normal direction is given by

$$y(\eta) = \frac{y_{max}\sigma\eta}{\eta_{max}\sigma + y_{max}(\eta_{max} - \eta)}. \tag{34}$$

Here, we choose $\sigma = 3.5$, and $y_{max} = \eta_{max} = 50$ (based on δ^*).

Both 2D ($\beta = 0$) and 3D ($\beta \neq 0$) cases are studied. Typical 3D results are shown in Figures 6 - 7. A $170 \times 34 \times 18$ grid is employed. We divide the whole computational domain into a physical domain and a buffer domain, the latter is one T-S wavelength long. Let $Re^* = 688$, $\omega_{2d} = \omega_{3d} = \omega = 0.075 (F = \omega/Re^* \times 10^6 = 109)$, and $\beta = 0.2$. The comparison of the amplitude distributions in both the wall-normal direction (eigenfunctions) and streamwise direction (amplifications) shows a good agreement with the LST results.

CASE	Fundamental (Figure 7 (a))
Re^*	1221.77
grids	$290 \times 34 \times 30$
length	16 λ_{TS} physical domain, 2 λ_{TS} buffer
height (based on δ^*)	50
time-step/T-S period	220
inflow disturbance	$\epsilon_{2d} = 0.0056$, $\epsilon_{3d} = 0.0004$
other parameters	$\beta = 0.2451$
	$\alpha_R = 0.2451$
	$\alpha_{R_{2d}} = 0.2690$
	$\omega_{2d} = \omega_{3d} = 0.0928$
	$\sigma = 4.05$
CASE	Subharmonic (Figure 7 (b))
Re^*	1221.77
grids	$338 \times 34 \times 26$
length	19 λ_{TS} physical domain, 2 λ_{TS} buffer
height (based on δ^*)	50
time-step/T-S period	220
inflow disturbance	$\epsilon_{2d} = 0.003$, $\epsilon_{3d} = 0.000125$
other parameters	$\beta = 0.178$
	$\alpha_R = 0.12965$
	$\alpha_{R_{2d}} = 0.2690$
	$\omega_{2d} = 0.0928$, $\omega_{3d} = 0.0464$
	$\sigma = 4.15$

Table 1. Parameters for transition over flat plate.

5.1.2 Whole process of transition over a smooth flat plate

To verify the ability of this code, further tests on a smooth flat plate were performed. Using the experimental input data of Saric et al.(1984), we did simulations for both the fundamental

breakdown and subharmonic breakdown. The inflow boundary condition is assumed to have the form of formula (33). The computational parameters are summarized in Table 1, and the results are shown in Figure 8. The numerical results match the experimental results very well.

5.2 Receptivity of flat-plate with an elliptic leading-edge

In this case, we set the Reynolds number based on the small axis of the ellipse $Re_h = 2400$. Figure 9 depicts the configuration considered here.

The base flow is characterized by large streamwise and normalwise velocity gradients around the leading-edge, and appearance of a maximum adverse pressure gradient exactly at the leading-edge-flat plate juncture. The boundary layer adjusts to recover to freestream pressure after an acceleration over much of the nose surface (mainly due to a strong favorable pressure gradient there). Figure 10 depicts results of the current base flow pressure gradient along the stagnation line and the wall surface, and that of Buter and Reed (1994) for comparison. They are in good agreement. The adverse peak value of the surface pressure gradient caused by body curvature changes at the juncture is considered to be one of the receptivity sources other than leading-edge (Goldstein & Hultgren,1989). It should be noted that a very small but almost constant adverse pressure gradient will amplify the instable mode once generated and after reaching the first branch of its neutral curve. Normal components of the base flow at the juncture and exactly the same downstream station shown in Figure 11 are found to agree well with that of Buter & Reed (1994). The boundary layer exhibits clearly a non-parallel characteristic which is not accounted for in the classic linear stability analysis.

The unsteady flow resembles a temporal and spatial evolution after an external harmonic vortical disturbance is imposed at the upstream boundary,

$$u(x_0, y, t) \;=\; \mathrm{Real}\{\epsilon_{enforce} A(|y| - y_c) e^{-\frac{(|y|-y_c)^2}{k}} e^{-i\omega t}\}, \tag{35}$$

where A is a parameter for adjusting the amplitude of enforced disturbance, ω is the frequency of the imposed disturbance, k is used to change the shape of u's profile, and y_c is the central point of the disturbance. Here, we use

$$\omega = 1.0, \quad k = 0.0075, \quad y_c = 0.15.$$

Note the disturbance is bounded very closely to the stagnation line of the base flow, as T-S waves are expected to be generated by a source term that is roughly the product of a Stokes

shear layer adjacent to the wall and the streamwise gradient of the mean-flow velocity(Goldstein & Hultgren, 1989). The boundary layer does involve a triple-deck structure after passing the leading-edge-flat plate juncture, and this can be seen from the instantaneous streamwise velocity component distributions at different distances from the wall after the 10th cycle of forcing (Figure 12). The response is evidently a complex combination of signals of varying wavelengths. The nature of the flow near the wall is influenced almost exclusively by the presence of T-S waves, while in the main inviscid region of the boundary layer convected disturbances dominate. Figure 13 shows the spatial evolution of the generated T-S wave (u component) aft of the pressure gradient maximum(at the juncture). The computed location of Branch I is about $x = 11.0$. A comparison of T-S amplification factor,

$$N = \log(A/A_0) \tag{36}$$

along the flat plate with that obtained by Buter & Reed (1994) is depicted in Figure 14. The current result is not as smooth as Buter & Reed, and one possibility is our input disturbance is not exactly the same as theirs. Also, from our simulation, we find the original convection wave (long wavelength wave) damps not as fast as that of Buter & Reed. Since this wave has the same frequency as the excited T-S wave, the amplification factor has some oscillations which involves the effects of the damping long wave.

The ratio of generated T-S wavelength to that of freestream disturbance wavelength is found to be around 0.40, and quite agreeable to the estimation by Goldstein(1983), which is $O(\epsilon)$ where $\epsilon = 0.39$ if calibrated by $Re_h^{-1/8}$. The receptivity coefficient is defined here as a convention by adopting the maximum rms-value of the disturbance at a location far upstream of the boundary layer. The level of receptivity in the current study at Branch I is 2.05%, while the same parameter in Buter & Reed (1994) is reported to be around 2.86-3.30%. This discrepancy may be due to the quantification of receptivity levels in the manner adopted, as the level of receptivity is more inherently related to some freestream disturbance which is varying dramatically along the boundary layer (Buter & Reed,1994). Note that the receptivity coefficient of the same geometry to freestream sound in Lin *et al.*(1992) is of the order 10^{-1}, much higher than both the above two computations.

5.3 Receptivity of 2D and 3D Joukowsky airfoils

The upstream boundary condition of the base flow at infinity is considered to be with zero attack angle, and the external freestream disturbance is introduced symmetrically to the axis of

the Joukowsky airfoil. This enables us to carry out simulations within the upper half of the flow field. Actually, all 2D and 3D results are obtained by the same code by assuming periodic spanwise boundary condition. The ratio of the half-thickness(h) of the airfoil to its chord-length(L) is 1/40, with the crest location about 1/4 of the chord-length. Other parameters for 2D and 3D simulations are listed in Table 2.

Similar to that of the flat plate with an elliptic leading-edge, the base flow of the present case has a strong favorable pressure gradient near the stagnation point; the boundary layer remains very thin until reaching the adverse pressure gradient regime. Except for a striking distinction near the trailing-edge of the airfoil, of which the influence we shall discuss later on, the present base flow differs from the former mainly in the surface pressure gradient distribution along the wall. Shown in Figure 15, the surface pressure gradient is positive everywhere, with its maximum value rather smaller than that in Figure 10. This is because the leading-edge aspect ratio is smaller (recall a comparison of 1/10 with 1/6), and the surface curvature discontinuity has been removed by smoothness of the Joukowsky airfoil.

	2D case	3D case
Re_L	1.6×10^5	1.8×10^5
L/h	40	36
grids	$482 \times 50 \times 4$	$402 \times 32 \times 26$
domain height	$25h$	$25h$
time-step/cycle of force	200	200
disturbance amplitude	$\epsilon_{\text{enforce}} = 0.01$	$\epsilon_{2d} = 0.02$, $\epsilon_{3d} = 0.02$
frequency	$\omega = 1.0$ ($F = 250$)	$\omega = 1.2$ ($F = 240$)

Table 2. Parameters for receptivity of 2D and 3D Joukowsky airfoils.

It is reasonable to guess, in this case, T-S waves will be present later along the wall and undergo a longer period of time of attenuation before enlarged. Figure 16(a) demonstrates the process of this development along a fixed grid line, $j = 5$, roughly equivalent to a height of $0.08h$ above the surface. T-S waves become observable only in the rear half of the airfoil, in contrast to an immediate appearance aft of the leading-edge juncture in the flat plate case. From Figure 16(b) we find the same complex combination of varying wavelength through the airfoil boundary layer, and the wavelength conversion as well. Again, the ratio of T-S wavelength to that of freestream disturbance is found to be about 0.40–not claimed here accurately because of variations of T-S wavelength itself.

With deferred onset of amplification of the most instable wave, the perturbation flow has a N factor(Figure 17) relatively small along the body surface. It grows much fast thereafter, and keeps increasing throughout the wake. This coincides with the above analysis of the disturbance velocity.

The 3D simulation is complemented by introduction of an external spanwise spatial harmonic disturbance(see Table 2) at the upstream boundary. From Figures 18 and 19 we can find that not only the 2D waves can be recepted after the disturbances pass the leading-edge region, but also the 3D oblique modes. The difference is that there is no wavelength conversion in the spanwise direction.

5.4 The whole process of transition around 3D Joukowsky airfoils

In this case, a Joukowsky airfoil with infinite width and zero attack angle is considered. The spanwise boundary condition is thus assumed to be periodic.

5.4.1 Enforced transition

We first investigate the process of enforced transition in a 2D Joukowsky airfoil boundary layer. In this case, the disturbance is imposed into the boundary layer directly. The associated parameters for numerical simulation are shown in Table 3, and the grids in (x, y)-plane are shown in Figure 20.

The simulation was carried out on an IBM RS 6000/590 workstation, and required approximately 100 hours of CPU time and 65 MB of memory.

Re_L	$126,000 (Re_h = 3,500)$
L/h	36
grids	$298 \times 34 \times 26$
domain height	$25h$
time-step/forcing cycle	250
disturbance amplitude	$\epsilon_{2d} = 0.01,\ \epsilon_{3d_\pm} = 0.005$
other parameters	$\omega = 0.7 (F = 228.6 \times 10^{-6})$
	$\beta = 1.0$
location of forcing	$x/h = 8.19$ (from the leading-edge)
points on the airfoil	214 (streamwise)

Table 3. Parameters for simulation of the whole process of transition over a Joukowsky airfoil (enforced transition).

The periodic disturbance is imposed at $x/h = 8.19$ (measured from the leading-edge). Though we still use formula (33), the distribution of the perturbation in the wall-normal direction can no

longer be called "eigenfunction". Figure 21 depicts the instantaneous contour plots of perturbation ω_x, ω_z, and $|\omega|$ on the $j = 6$ ($\approx 0.07h$ from the wing surface) grid surface after the 10th cycle of forcing.

Figure 22 gives a response to the flow field which is subject to the periodic disturbance input at the imposed location. It is quite clear that as the perturbation waves travel downstream, the nonlinear affection increases. At some downstream location, the sign of randomness appears, and the so-called spikes can be observed. The flow field is no longer periodic.

5.4.2 Natural transition

In this case, a similar configuration as in the above subsection is investigated. Now, the disturbance is not imposed directly into the boundary layer, but from free-stream. The pattern of disturbance is still the same: one 2D wave and two oblique waves. The parameters used in this simulation are listed in Table 4.

Re_L	$200,000 (Re_h = 5000)$
L/h	40
grids	$402 \times 32 \times 26$
domain height (based on h)	25
time-step/cycle of forcing	200
disturbance amplitude	$\epsilon_{2d} = 0.02,\ \epsilon_{3d} = 0.02$
other parameters	$\omega = 1.2 (F = 240 \times 10^{-6})$
	$\beta = 1.0$
points on the airfoil	322 (streamwise)

Table 4. Parameters for simulation of the whole process of transition over a Joukowsky airfoil (natural transition).

The simulation was carried out on an IBM RS 6000/590 workstation, and required approximately 150 hours of CPU time and 124 MB of memory to run 18 forcing periods.

The periodic disturbance is imposed at $x/h \approx -15$ from the leading-edge. Figure 23 depicts the instantaneous contour plots of perturbation ω_x, ω_z, and $|\omega|$ on the $j = 5$ ($\approx 0.07h$ from the wing surface) grid surface after the 17th cycle of forcing. Figure 24 gives a response to the flow field which is subject to the periodic disturbance input at inflow. It is quite clear that different from the previous case, this case includes a wavelength conversion process. According to Buter and Reed (1994), the receptivity coefficient for the freestream vorticity receptivity is affected by the aspect ratio of the leading-edge and continuity of surface curvature. In this study, there is no curvature discontinuity on the wall surface, and the aspect ratio of the leading-edge is quite large

(about 1:10), thus the receptivity coefficient is very small. Nevertheless, we still observed the nonlinear breakdown at some downstream location: the sign of randomness appears, the so-called spikes can then be observed, the flow field is no longer periodic in time, and the vortex breakdown appears.

Figure 25 depicts the contour plots of total ω_z at both peak and valley planes during the 17th forcing period. Though the process is quite similar to that of the previous case, the breakdown location was delayed because the amplitude of effective T-S wave induced from receptivity is very weak.

There is no doubt the current numerical simulation has already provided a clear picture of the transition process with relatively coarse grid and medium Reynolds number.

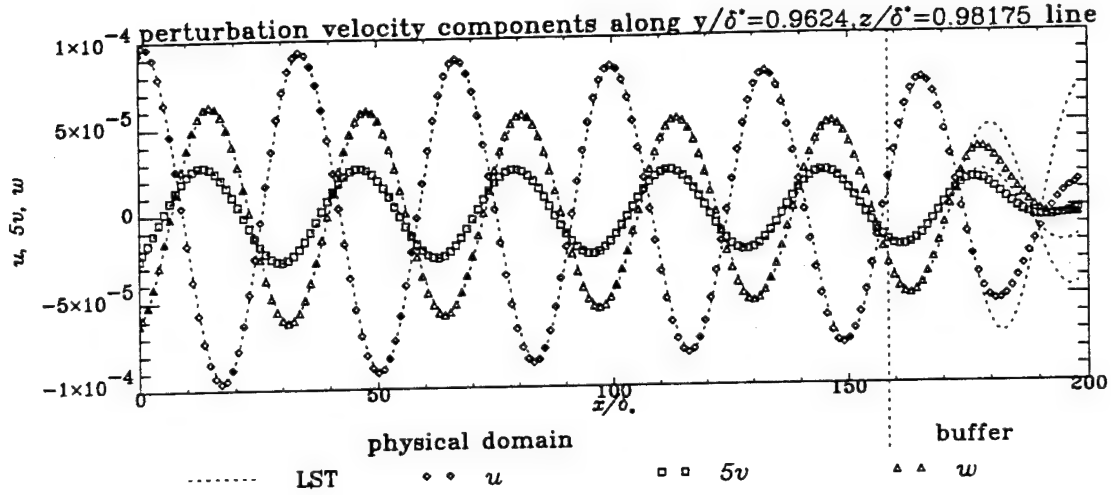

Figure 6. Amplitude of u, v, and w distribution at $t = 6T$.

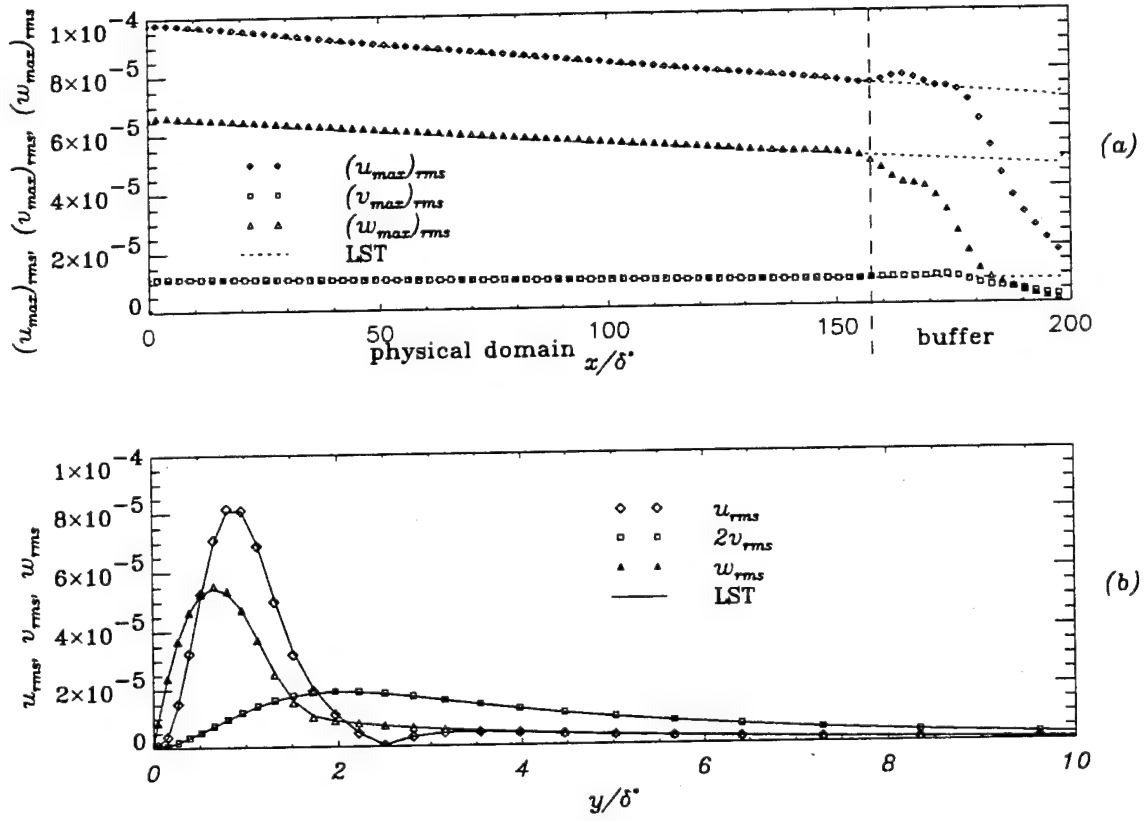

Figure 7. (a) Comparison of the maximum u, v, and w amplitudes with LST. (b) Comparison of the numerical and LST profiles of velocity at $x/\delta^* = 114.91$ (3D case).

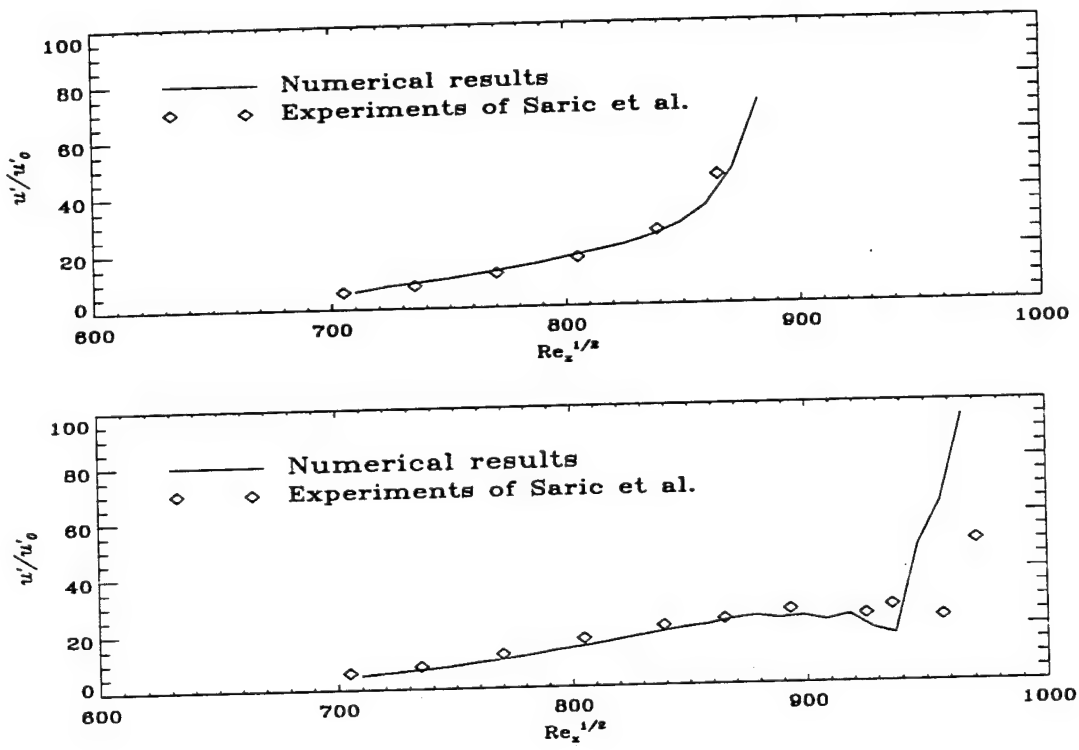

Figure 8. (a) Comparison of normalized perturbation velocity amplitude against $Re_\delta (= Re_x^{1/2})$ with experimental results of Saric et al. (1984) for the fundamental breakdown case. (a) Comparison of normalized perturbation velocity amplitude against Re_δ at $u = 0.4$ with experimental results of Saric et al. (1984) for the subharmonic breakdown case.

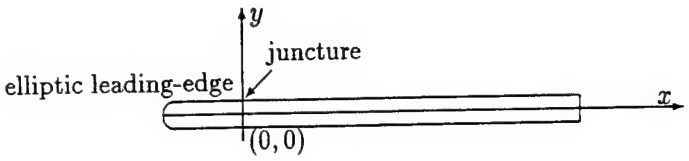

Figure 9. Sketch of a flat plate with an elliptic leading-edge.

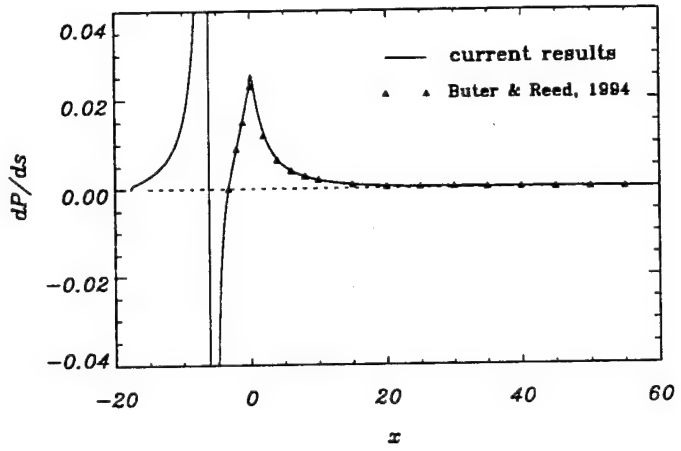

Figure 10. Base flow surface pressure gradient of the flat-plat with an elliptic leading-edge.

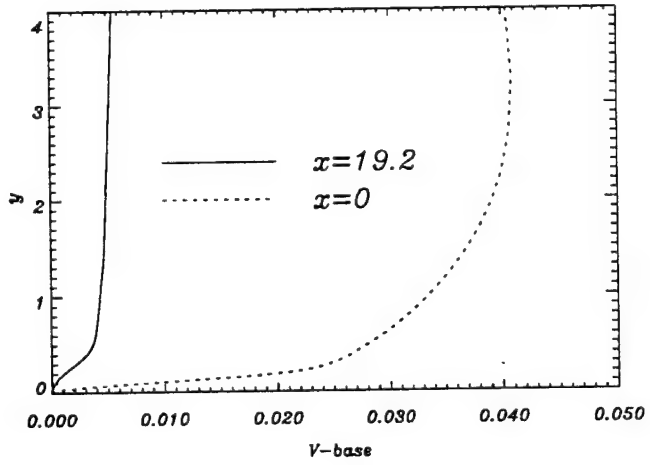

Figure 11. Base flow normal velocity profile at x=0, and x=19.2.

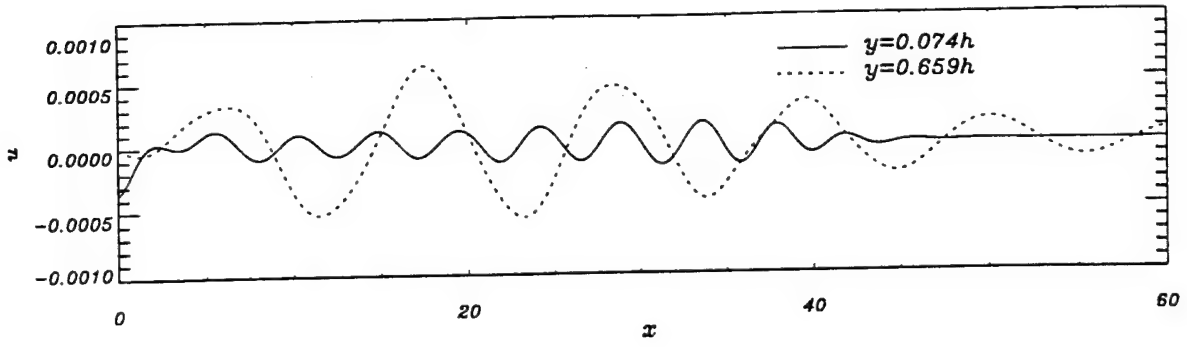

Figure 12. Instantaneous perturbation u distribution after 10th cycle of forcing.

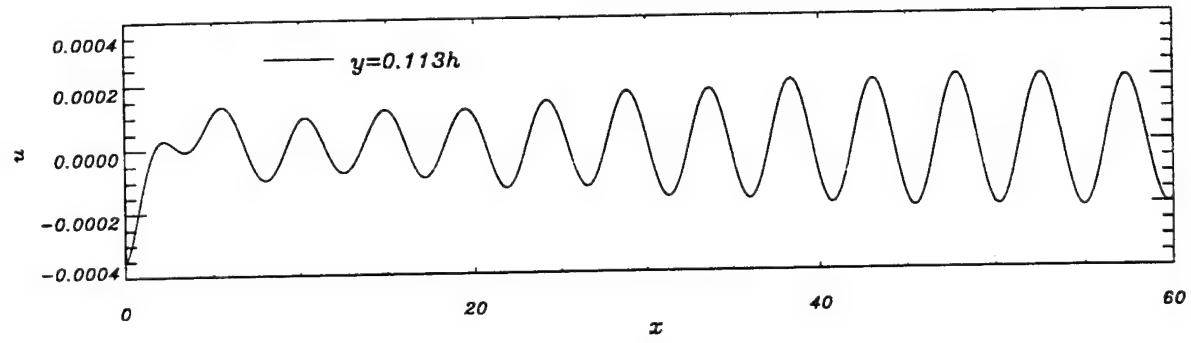

Figure 13. Spatial evolution of generated $T - S$ waves.

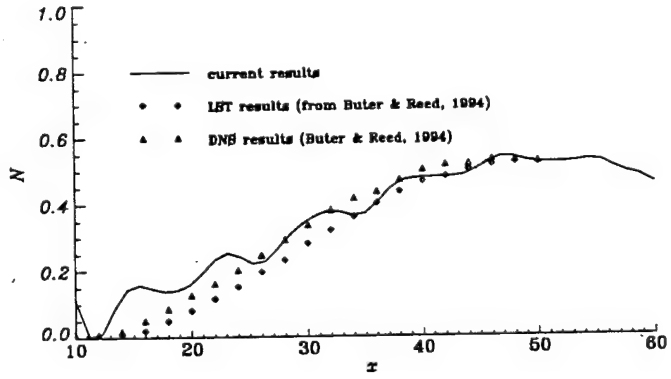

Figure 14. Computed perturbation amplification factor.

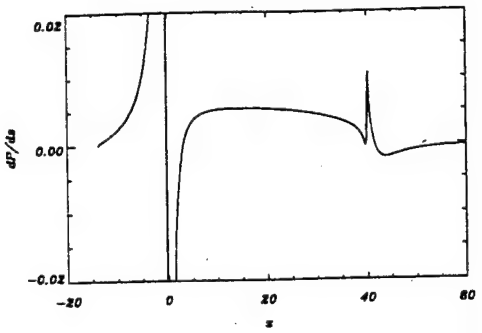

Figure 15. Base flow surface pressure gradient for the 2D Joukowsky airfoil.

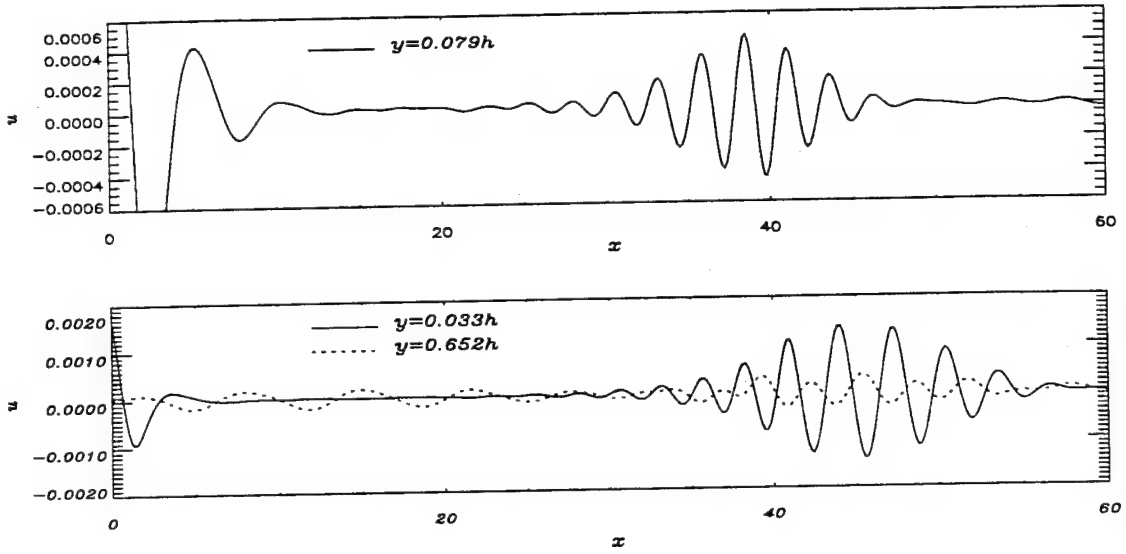

Figure 16. (a) Spatial evolution of generated unsteady waves along fixed grid line after 10th cycle of forcing. (b) Instantaneous perturbation u distribution along two grid lines after 14th cycle of forcing.

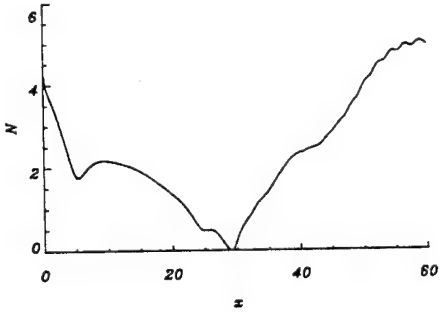

Figure 17. Computed perturbation amplification factor for the 2D Joukowsky airfoil.

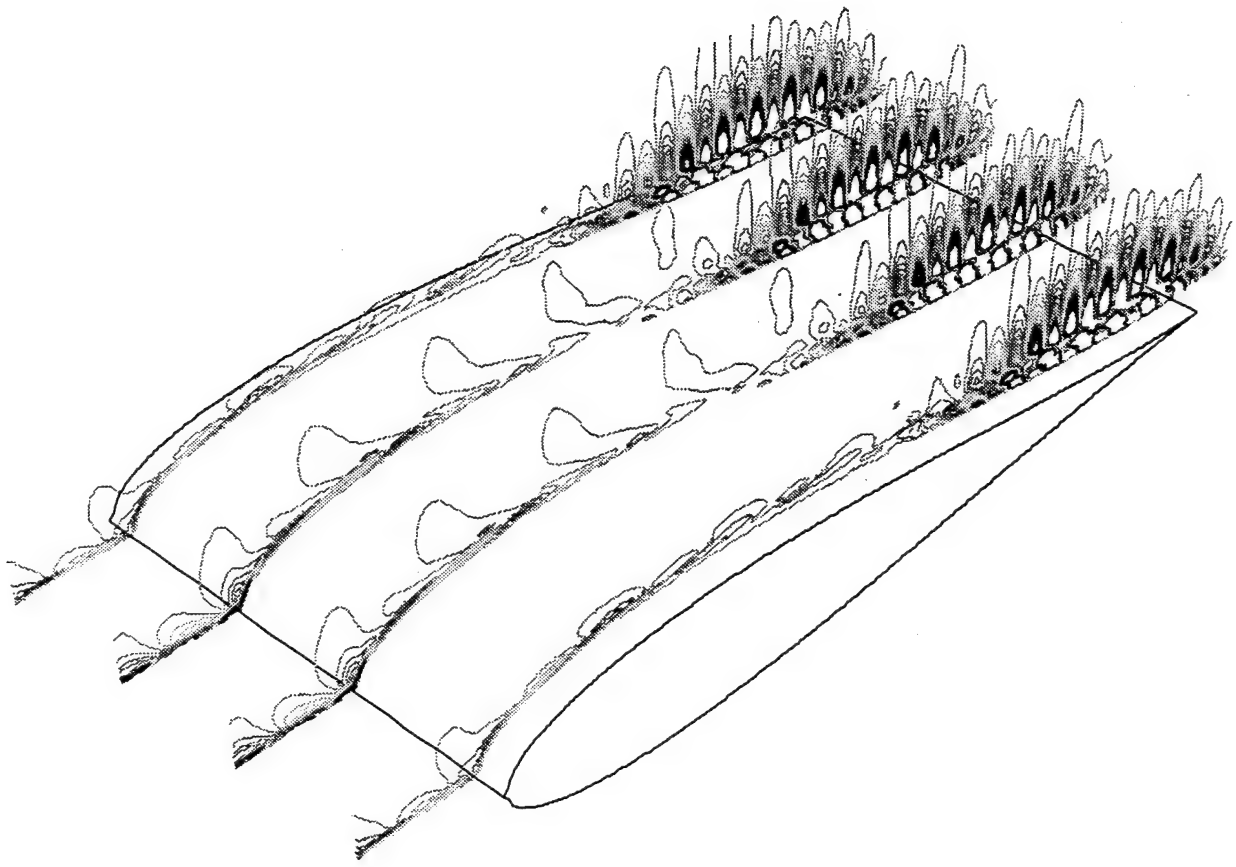

Figure 18. Perturbation u distribution after 14th cycle of forcing over the 3D Joukowsky airfoil.

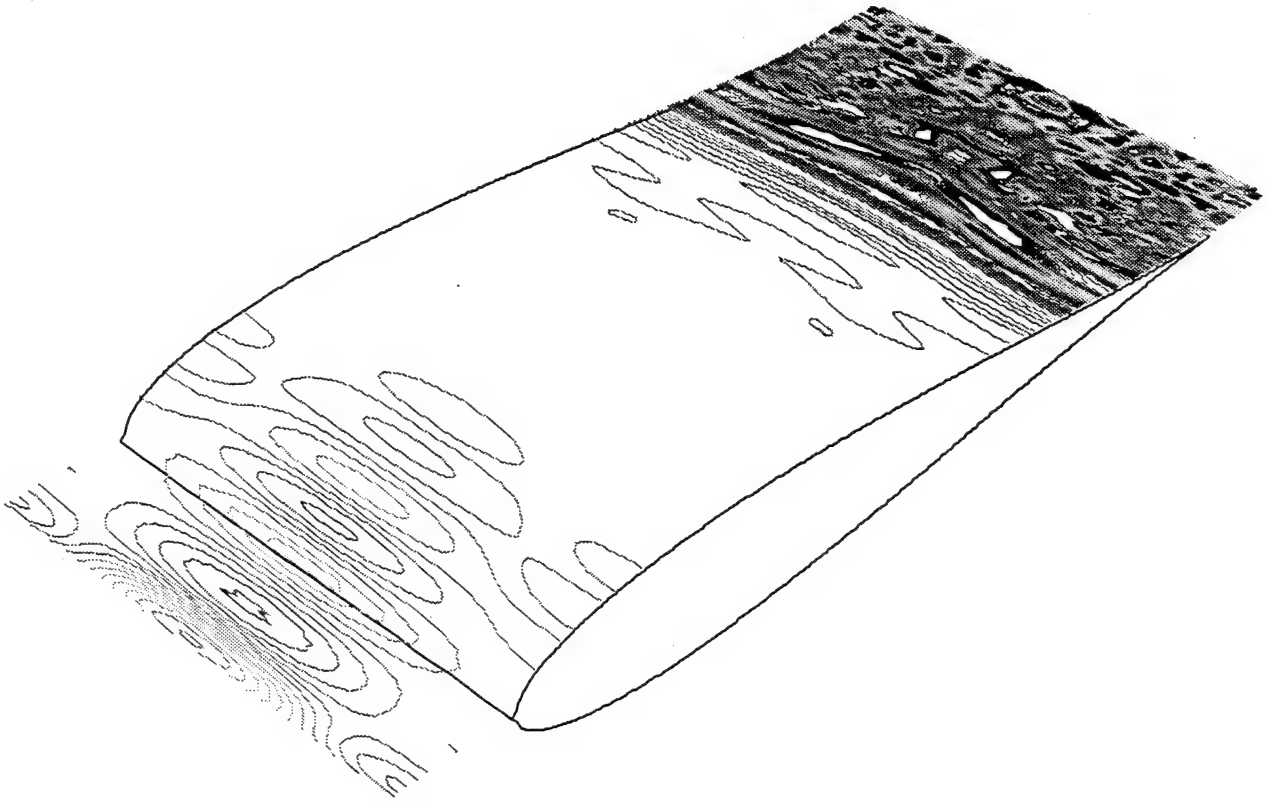

Figure 19. Wall surface spanwise perturbation vorticity contour over the 3D Joukowsky airfoil(at $t = 16T$).

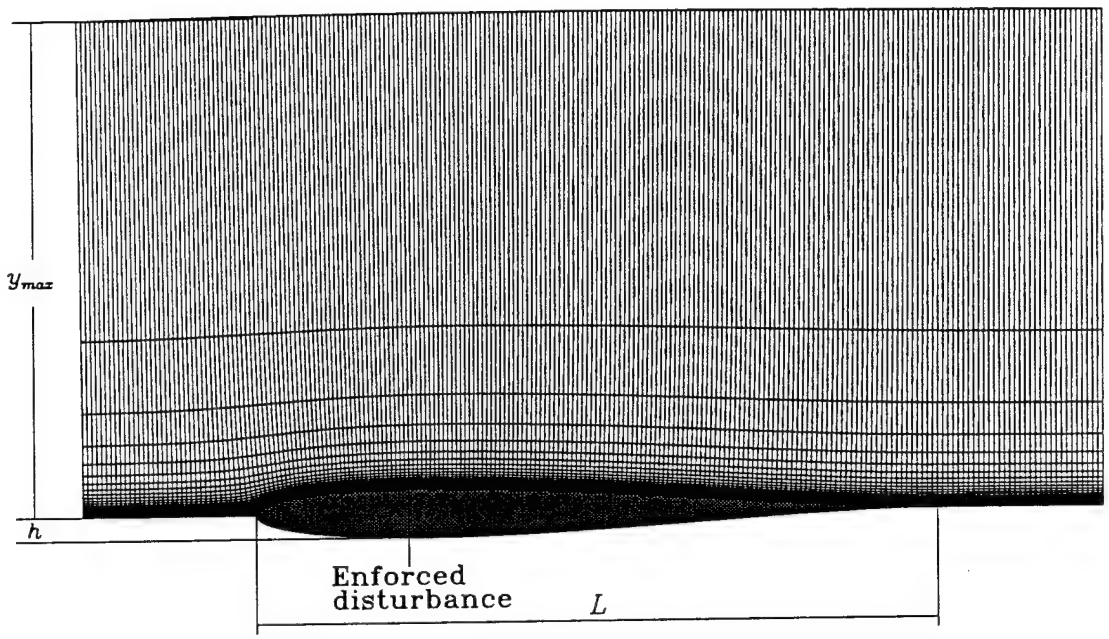

Figure 20. Grids for the Joukowsky airfoil in the (x, y)-plane.

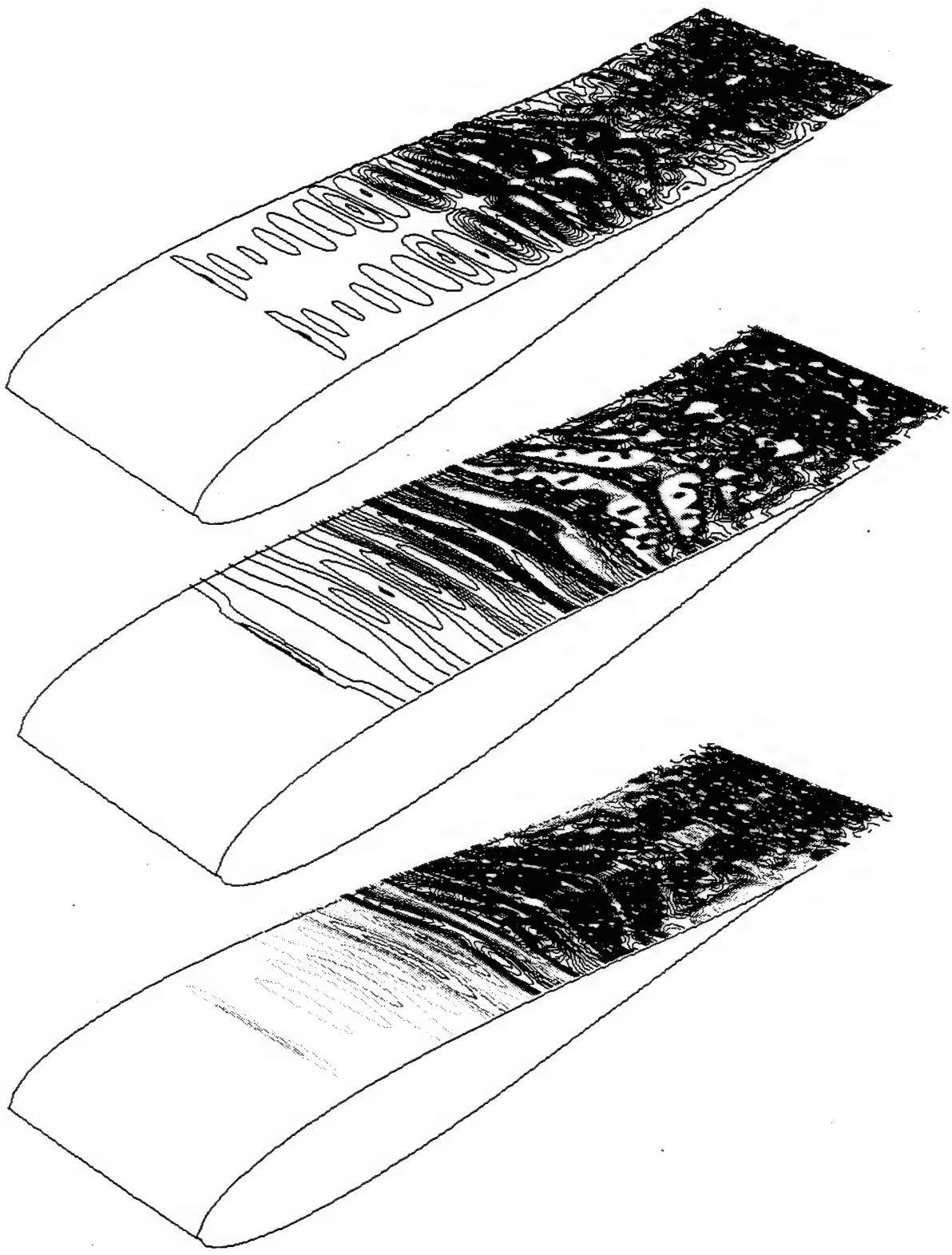

Figure 21. Instantaneous contour plots of perturbation ω_x, ω_z, and $|\omega|$ on the $j = 6$ ($\approx 0.06h$ from wall surface) grid surface at $t = 10T$ for the enforced transition case.

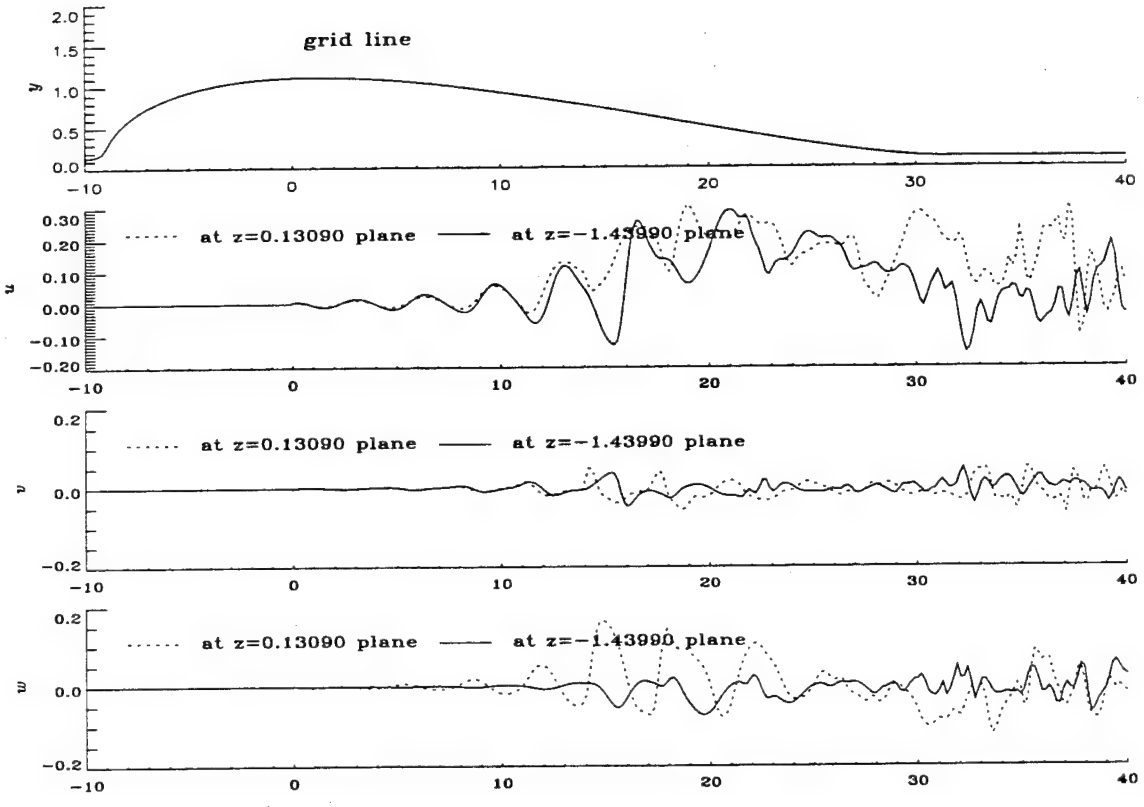

Figure 22. Instantaneous disturbance velocity components at $t = 10T$ along a grid line ($\approx 0.07h$ from the wing surface) for the enforced transition case.

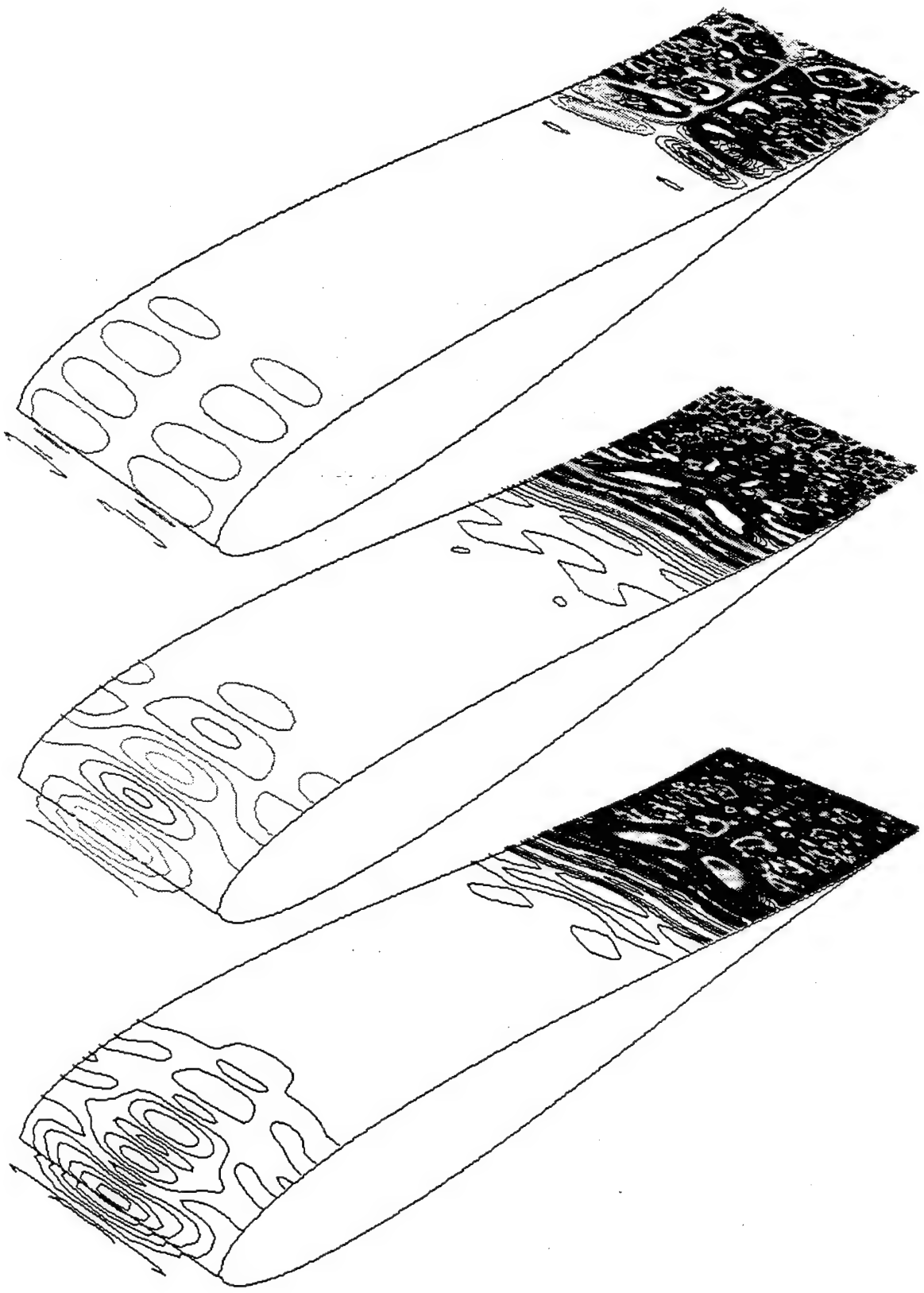

Figure 23. Instantaneous contour plots of perturbation ω_x, ω_z, and $|\omega|$ on the $j = 6$ grid surface at $t = 17T$ for the natural transition case.

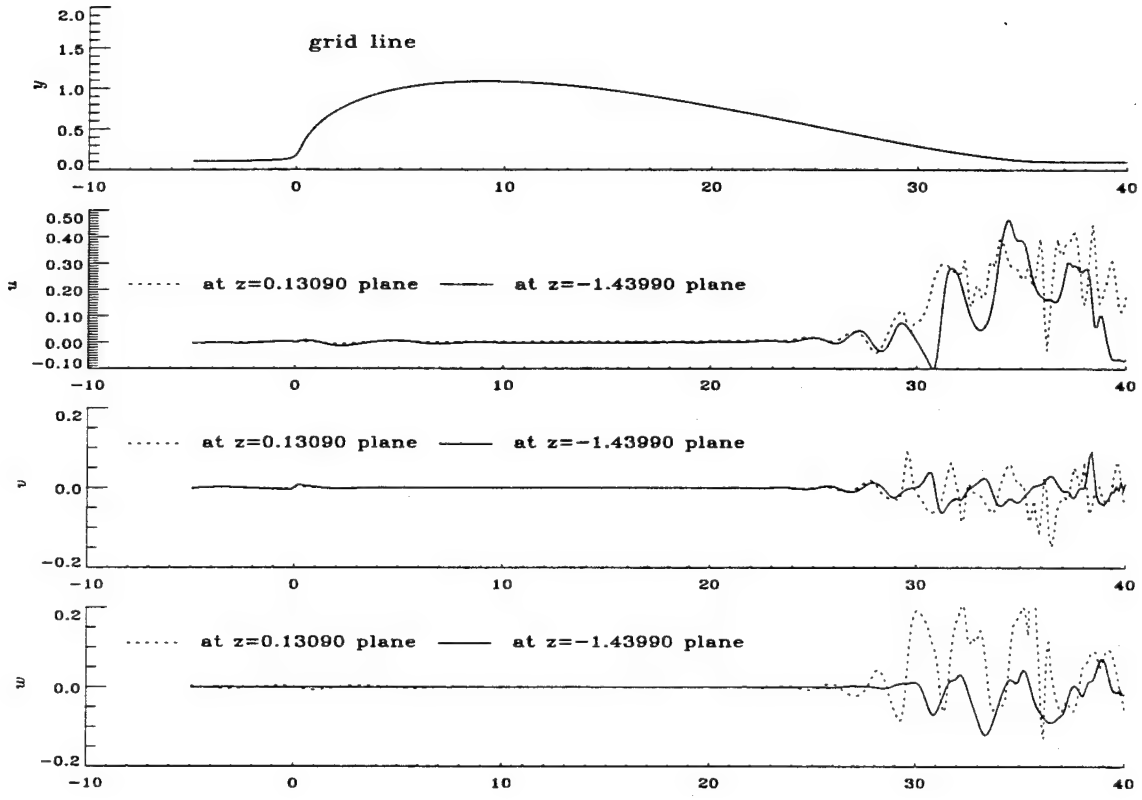

Figure 24. Instantaneous disturbance velocity components at $t = 17T$ along a grid line ($\approx 0.7h$ from the wing surface) for the natural transition case.

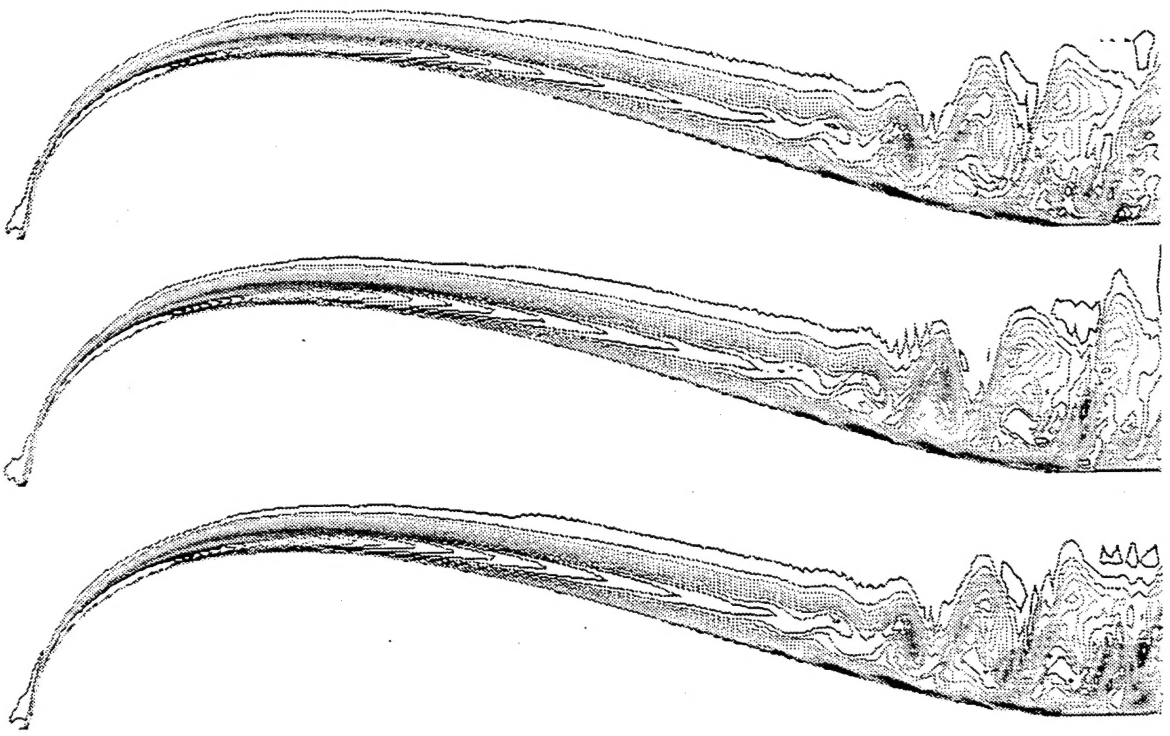

Total ω_z on the $z = -0.1309$ plane at $t = 16T, 16.5T, 17T$.

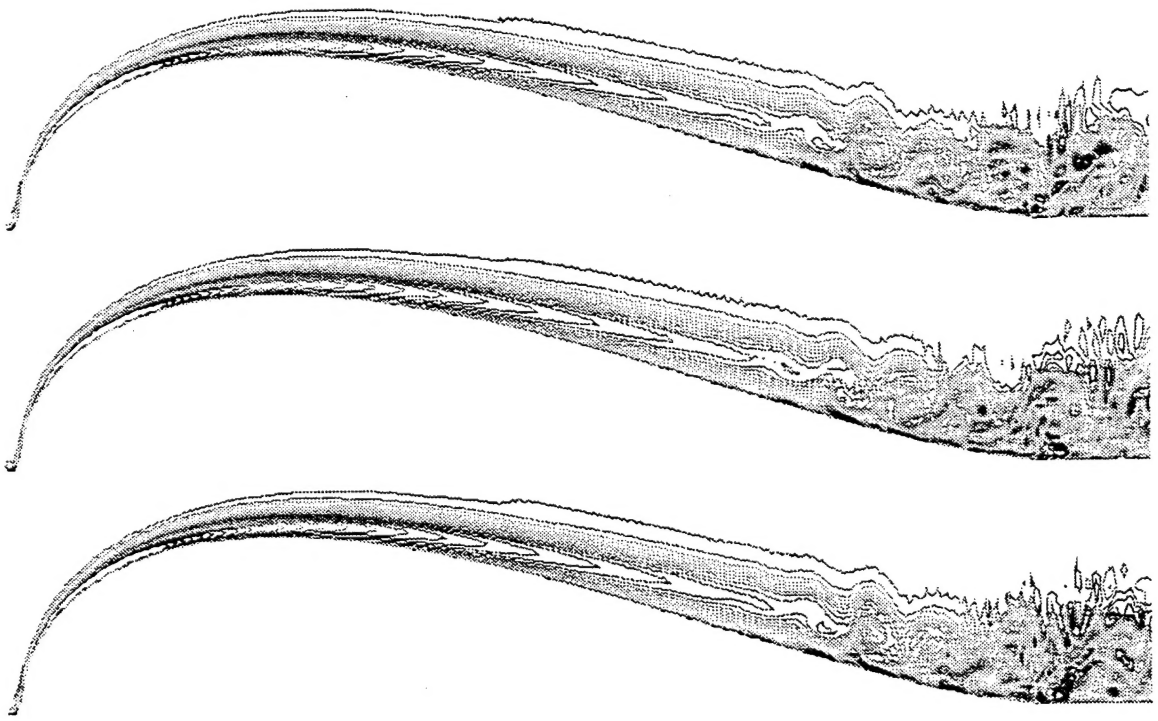

Total ω_z on the $z = -1.7017$ plane at $t = 16T, 16.5T, 17T$.

Figure 25. Instantaneous contour plots of total ω_z on the $z = -0.1309$ and $z = -1.7017$ planes during the 17th forcing period for the natural transition case.

6 Concluding Remarks

From the above discussion, we can conclude

- The current numerical approach can handle fairly complicated geometries by using the high-order grid transformation.
- The wavelength conversion has been numerically simulated, showing out capability to simulate more practical cases of natural and enforced transition.
- 3-D simulation for receptivity and transition basically works. We can use a rather coarse grid to study the behavior of most energetic eddies, and describe some physics of transition which may help the experimental and theoretical works.
- For the realistic problem, the memory size and CPU cost will increase further, so a code under parallel architecture needs to be developed soon.

7 Acknowledgment

This work is supported by AFOSR/NA under grant No. F49620-95-1-0018. The authors are grateful to Dr. L. Sakell and AFOSR for the support. The authors wish to thank DoD HPC for providing CRAY-C90 and SP2 time for this study.

References

[1] *Special Course on Skin Friction Drag Reduction, AGARD Report* 786, Mar. 1992.

[2] *Progress in Transition Modelling, AGARD Report* 793, Mar. 1993.

[3] Brandt, A., *Multigrid techniques: Guide with application to fluid dynamics.* GMD Studie, GMD, St. Augustine, 1984.

[4] Buter, T.A. and Reed, H.L., Boundary layer receptivity to free-stream vorticity, *Phys. Fluids*, vol.6, no.10, pp.3368, 1994.

[5] Goldstein, M.E., The evolution of Tollmien-Schlichting waves near a leading edge, *J. Fluid Mech.* **127**, pp.959-981, 1983.

[6] Goldstein, M.E., Scattering of acoustic waves into Tollmien-Schlichting waves by small stream-wise variation in surface geometry, *J. Fluid Mech.* **154** pp.509-529, 1985.

[7] Goldstein, M.E. and Hultgren, L.S., Boundary-layer receptivity to long-wave free-stream disturbances. *Ann. Rev. Fluid Mech.* **21**, 137-66, 1989.

[8] Kleiser, L. and Zang, T.A., Numerical simulation of transition in wall-bounded shear flows, *Ann. Rev. Fluid Mech.*, vol.23, pp.495, 1991.

[9] Lin, N., Reed, H.L., and Saric, W.S., Effect of leading-edging geometry on boundary-layer receptivity to freestream sound. *Instability, Transition and Turbulence*, ed. M.Y., Hussaini, A. Kumar and C.L., Streett, Springer-Verlag, 1992.

[10] Liu, C., Liu, Z., and McCormick, S., Multigrid methods for flow transition in planar channel, *Comput. Phy. Comm.*, vol.65, pp.188, 1991.

[11] Liu, Z. and Liu, C., Fourth order finite difference and multigrid methods for modelling instability in flat plate boundary layers, *J. Comput. Wind. Eng.*, vol.52, pp.412, 1992.

[12] Liu, C., Liu, Z., and McCormick, S., Multigrid Methods for Flow Transition in Three-Dimensional Boundary Layers with Surface Roughness, *NASA Contractor Report* 4540, Sep. 1993.

[13] Liu, C. and Liu, Z., High order finite difference and multigrid methods for spatially-evolving instability. *J. Comput. Phys.*, **106**, 92-100, 1993.

[14] Liu, Z. and Liu, C., Fourth order finite difference and multigrid methods for modelling instability in flat plate boundary layers–2D and 3D approaches, *Comput. Fluids*, vol.23, no.7, pp.955, 1994.

[15] Liu, C. and Liu, Z., Multigrid mapping and box relaxation for simulation of the whole process of flow transition in 3D boundary layers *J. Comput. Phys.*, **119**, 325-341, 1995.

[16] Morkovin, M.V., On the many faces of transition, *Viscous Drag Reduction*, ed. C.S.Wells, Plenum, 1969.

[17] Patankar, S.V. and Spalding, D.B., A Calculation Procedure for Heat, Mass and Momentum Transfer in 3-Dimensional Parabolic Flows. *Int. J. Heat Mass Transfer* **15**, 1787-1806, 1972.

[18] Reed, H.L., Direct numerical simulation of transition: The spatial approach, *Progress in Transition Modelling, AGARD Report* 793, Mar. 1993.

[19] Saric, W.S. and Reed, H.L., Leading edge receptivity to sound: Experiments, DNS and Theory, *AIAA 94-2222*, 1994.